Molecular Cancer

RESEARCH

Open Access

Co-targeting of epigenetic regulators and BCL-XL improves efficacy of immune checkpoint blockade therapy in multiple solid tumors

Yaiza Senent[1,2,3], Vicente Fresquet[2,4†], Victoria Jiménez[2,4†], Karmele Valencia[1,2,3,5], Francisco Exposito[1,2,5,6], Patxi San Martín-Úriz[2,4], Gracián Camps[1], Eva Fernández-Pierola[1], Borja Ruiz-Fernández de Córdoba[1], Marisol González-Huarriz[1,2,7], Ibon Tamayo[8], Ana Remírez[1,2,5], Haritz Moreno[1], Diego Serrano[1,2,5,6], Daniel Ajona[1,2,3,5], Marta M. Alonso[1,2,7], Fernando Lecanda[1,2,5,6], Antonio Pineda-Lucena[9], Felipe Prósper[2,4,5,10], Miguel F. Sanmamed[1,2,5,11], Alfonso Calvo[1,2,5,6], Jose A. Martinez-Climent[2,4,5*] and Ruben Pio[1,2,3,5*]

Summary

Epigenetic modulators in combination with proapoptotic drugs have become the standard of care treatment in hematological malignancies. Conversely, these combinations have failed to demonstrate clinical efficacy in solid tumors. To address this discrepancy, we conducted a comprehensive analysis of the anti-tumor activity of epigenetic inhibitors in combination with BH3 mimetics that block anti-apoptotic proteins BCL-XL, BCL2 or MCL1 in a large set of solid tumor cell lines derived from patients and mouse models. Treatment with epigenetic drugs targeting DNA methyltransferase, histone methyltransferase, and histone deacetylase enzymes in combination with a BCL-XL inhibitor resulted in marked synergistic in vitro responses both in human and mouse solid tumor cell lines. This unique BCL-XL dependency was in clear contrast to hematological malignancies, which are largely dependent on BCL2 or MCL1 inhibition under epigenetic drug treatment. Mechanistically, co-targeting of epigenetic regulators and BCL-XL induced expression of endogenous retroelements that led to immunogenic cell death. We thus hypothesized that this response may sensitize tumor cells to immune checkpoint blockade (ICB). Accordingly, treatment with a triple combination of epigenetic and BCL-XL inhibitors with an anti-PD-1 monoclonal antibody in vivo reduced tumor growth and prolonged overall survival in a panel of murine syngeneic and orthotopic models of lung, colorectal and breast carcinomas, melanoma, and glioblastoma, as well as in an immunocompetent human colon cancer model. Using flow cytometry and single-cell RNA sequencing of the tumor microenvironment, we found that the broad activity of the triple therapy relied on the expansion of T and NK cells with cytotoxic potential, an increase in the M1/M2 macrophage ratio, and a reduction of immunosuppressive Treg cells, dendritic cells, and B lymphocytes. In

†Vicente Fresquet and Victoria Jiménez contributed equally to this work.

*Correspondence:
Jose A. Martinez-Climent
jamcliment@unav.es
Ruben Pio
rpio@unav.es
Full list of author information is available at the end of the article

© The Author(s) 2025. **Open Access** This article is licensed under a Creative Commons Attribution-NonCommercial-NoDerivatives 4.0 International License, which permits any non-commercial use, sharing, distribution and reproduction in any medium or format, as long as you give appropriate credit to the original author(s) and the source, provide a link to the Creative Commons licence, and indicate if you modified the licensed material. You do not have permission under this licence to share adapted material derived from this article or parts of it. The images or other third party material in this article are included in the article's Creative Commons licence, unless indicated otherwise in a credit line to the material. If material is not included in the article's Creative Commons licence and your intended use is not permitted by statutory regulation or exceeds the permitted use, you will need to obtain permission directly from the copyright holder. To view a copy of this licence, visit http://creativecommons.org/licenses/by-nc-nd/4.0/.

conclusion, we report a novel regimen combining epigenetic and BCL-XL inhibitors with ICB that produces potent anti-tumor responses in multiple preclinical models of solid tumors.

Keywords Solid tumors, Epigenetic modulators, CM272, Anti-apoptotic proteins, BCL-XL, A1331852, Immune checkpoint blockade, Anti-PD-1

Introduction

Therapeutic targeting of epigenetic enzymes has revolutionized the treatment of hematological malignancies. Eight inhibitors of DNA methyltransferases (DNMTs), histone methyltransferases (HMTs) and histone deacetylases (HDACs) have been approved for the treatment of patients with myeloid and lymphoid malignancies, and some others are being evaluated in clinical trials. However, epigenetic agents have poor pharmacokinetic and safety profiles, primarily due to lack of specificity, which limits their efficacy as single agents. Furthermore, in marked contrast to hematological malignancies, epigenetic agents have not demonstrated efficacy in most solid tumors [1–4]. In fact, only two agents have been approved by the FDA for the treatment of two rare cancers, cholangiocarcinoma and epithelioid sarcoma [5]. Accordingly, clinical development of epigenetic drugs for solid tumors is underway in combination with other anticancer treatments, including targeted agents, chemotherapy, radiotherapy or immunotherapy [6].

Inhibition of epigenetic enzymes in tumor cells induces the transcription of epigenetically silenced endogenous retroelements, such as endogenous retroviruses (ERVs) [7–12]. Retroelement transcription generates double-stranded RNAs (dsRNAs) that trigger viral mimicry responses initiated by RIG-I and MDA5 helicases [13]. These helicases activate the downstream adaptor protein MAVS to promote interferon (IFN) signaling [8, 14]. In turn, IFN responses increase tumor immunogenicity, which sensitizes tumor cells to immune checkpoint blockade therapy [8, 15–17]. Accordingly, epigenetic agents in combination with programmed cell death protein 1 (PD-1)/programmed cell death ligand 1 (PD-L1) targeting drugs are being clinically tested in solid tumors [18, 19]. Unfortunately, clinical trials have not shown encouraging results [20–22]. More effective combinations may emerge from a better understanding of the mechanisms by which solid tumors respond poorly to epigenetic agents.

Following epigenetic therapy, dsRNA recognition by helicases depletes intracellular ATP, reversing the Warburg effect and increasing cancer cell dependence on aerobic glycolysis. This is associated with hyperactivation of mitochondrial oxidative phosphorylation (OXPHOS), which generates excessive reactive oxygen species and leads to caspase-independent tumor cell death [23]. Such constitutive OXPHOS state renders tumor cells susceptible to inducers of mitochondrial apoptosis including the BCL2 inhibitor venetoclax [23, 24]. Thus, the DNMT inhibitors azacitidine or decitabine in combination with venetoclax have been approved for the treatment of patients with newly diagnosed acute myeloid leukemia (AML) [25].

Here, we present a comprehensive analysis of the potential synergistic effect of pro-apoptotic agents in combination with epigenetic drugs in solid tumors, with particular focus on lung cancer, the leading cause of cancer-related deaths worldwide. Human and mouse solid tumor cell lines were inherently resistant to agents targeting anti-apoptotic proteins; however, epigenetic agents universally synergized with inhibitors of BCL-XL to promote cancer cell apoptosis. This observation was in marked contrast to hematological malignancies, which are sensitized to epigenetic agents by BCL2 or MCL1 inhibitors. Mechanistically, we found that co-targeting epigenetic enzymes and BCL-XL increased immunogenic cell death, which sensitized solid tumors to anti-PD-1 blockade in vivo, resulting in profound anti-tumor responses in mouse and human models of various solid cancers. This study presents a novel therapeutic combination that reinstates the potential of epigenetic therapeutics to treat and cure patients with solid tumors.

Materials and methods

Cell lines

The human and mouse cancer cell lines used in the study are listed in Supplementary Table 1. Unless otherwise indicated, cells were cultured in RPMI-1640 supplemented with Glutamax (Gibco), 10% Fetalclone (Thermo Fisher Scientific), 100 U/mL penicillin and 100 µg/mL streptomycin (Invitrogen). All cell lines were routinely tested for *Mycoplasma*. The IC_{50} values of the epigenetic agents CM272, vorinostat and azacitidine in some of these cell lines are shown in Supplementary Table 2.

Reagents

The epigenetic drugs azacitidine and vorinostat were purchased from Selleckchem, while CM272, a reversible dual small molecule that inhibits G9a and DNMTs, was synthesized as described previously [26]. The proapoptotic drugs A1331852 (a BCL-XL inhibitor), venetoclax (a BCL2 inhibitor) and S63845 (an MCL1 inhibitor) were

purchased from Selleckchem and ChemieTek. The anti-PD-1 humanized antibody pembrolizumab was obtained from Merck, and the monoclonal antibody against mouse PD-1 was obtained from BioXCell (clone RMP1-14). The other antibodies used in this study are listed in Supplementary Table 3.

Cell viability

Cells were seeded in 96-well culture plates at a density of 2 to 3×10^3 cells/well and treated with the different epigenetic or proapoptotic drugs, alone or in combination, for 24 to 48 h. Cell viability was quantified using the Deep Blue Cell Viability Kit (BioLegend). Fluorescence was quantified using a Vorinoskan Flash (Thermo Scientific) and analyzed using SkanIt software 2.4.3. All experiments were performed in triplicate.

Cell death analysis

Cells were seeded in 12-well culture plates at a density of 7.5×10^4 cells/well and treated with the different epigenetic or proapoptotic drugs, either alone or in combination, for 24 h. Following treatment, cells were trypsinized and washed with PBS.

For cell death analysis, cells were resuspended in 100 µl of annexin binding buffer (BD Bioscience) and stained with 1 µl of APC Annexin V (Biolegend) and 1 µl of propidium iodide (Sigma-Aldrich). Cells were incubated in the dark at room temperature for 15 min. After the incubation, 400 µl of binding buffer was added, and cells were analyzed by flow cytometry using a FACS Canto II flow cytometer (BD Biosciences). Data were processed using FlowJo v10.7.1 software.

Caspase 3/7 activity was measured using the Cell Event Caspase 3/7 Green Flow Cytometry assay kit (ThermoFisher). Cells were resuspended in 1 ml of PBS with 2% BSA. After the addition of 1 µl of detection reagent, cells were incubated at 37°C for 30 min. In the final 5 min of incubation, 1 µl of 7-AAD was added. Flow cytometry analysis was conducted as described above.

For calreticulin translocation measurement, cells were washed with PBS and incubated with a rabbit polyclonal anti-calreticulin antibody (Abcam) in PBS with 2% BSA for 30 min at 4°C. Following incubation, cells were washed and incubated with a secondary goat anti-rabbit antibody conjugated to Alexa Fluor 647 (Invitrogen) in PBS with 2% BSA for 30 min at 4°C. Cells were analyzed by flow cytometry as described above.

For MHC-I and PD-L1 detection, cells were harvested, washed with PBS, and incubated with antibodies against MHC-I (APC mouse anti-human HLA-ABC clone G46-2.6 or PE rat anti-mouse CD274 clone MIH5, BD Pharmagen) or PD-L1 (PE/cyanine7 anti-human CD274 clone 29E.2 A3 or APC anti-mouse H-2Db clone KH95, Biolegend) for 30 min at 4°C. Flow cytometry data acquisition and analysis were performed as described above.

Real-time PCR

Total RNA was isolated using Tri reagent (Sigma-Aldrich) followed by DNase I (Thermo Fisher Scientific). cDNA was synthesized using random primers and M-MLV reverse transcriptase (Invitrogen) according to the manufacturer's protocol. Relative gene expression was determined by real-time PCR using gene-specific primers and SYBR Select Master Mix (Applied Biosystems) on a ViiA 7 Real-Time PCR System (Applied Biosystems). Gene expression was analyzed by the $2^{-\Delta\Delta Ct}$ method by normalizing the expression of each gene to PGK1 and then to the control. Primers for real-time PCR are listed in Supplementary Table 4. All experiments were performed in triplicate.

Western blotting

Tumor cells (2×10^5 cells/well in 6-well plates) were treated with the corresponding drug for 24 h. Western blot analyses were performed as previously described [23], and quantified using ImageJ software. Antibodies are listed in Supplementary Table 4.

Measurement of ADP/ATP, extracellular acidification and oxygen consumption rates

ADP and ATP levels were quantified using the ADP/ATP Ratio Assay Kit (Sigma Aldrich) in cultured cells treated with different concentrations of the drugs for 24 h. Extracellular acidification rate (ECAR) and oxygen consumption rate (OCR) were quantified in an XF24 Extracellular Flux Analyzer (Seahorse Biosciences) as previously described [23]. In addition, OCR was quantified using the OCR-ST-96 WELL kit fluorometric assay (Oxoprobics).

Mouse cancer models and therapeutic schedules

FVB/N, C57BL/6 J and BALB/c mice were purchased from Envigo. Sv/129 mice were obtained from Janvier. All animal experiments were performed in accordance with the protocols approved by the institutional animal care committee (references 049–18 and 131–22).

LLC cells (2×10^6) were injected subcutaneously into the flanks of 8–12 week old female C57BL/6 J mice. Tumor-bearing mice were treated with vehicle, 5 mg/kg CM272 (i.p.; 5 days per week, starting on day 6), 100 µg anti-PD-1 (i.p.; days 7, 10 and 14) and/or 5 mg/kg A1331852 (i.p.; 3 days per week starting on day 7). For the orthotopic LLC model, 6–8 week old female C57BL/6 J mice were anesthetized with 2% isoflurane and placed in lateral decubitus position. 1×10^5 LLC-luc cells in 10 µL medium/Matrigel (Corning) (1:1) were injected directly

into the left lung lobe. Tumor growth was measured once or twice weekly by bioluminescence using a real-time in vivo system (PhotonImager, Biospace Laboratory). On day 5 postinjection, mice were randomized according to tumor volume and treated with vehicle, CM272 (5 days per week starting on day 5), anti-PD-1 (days 7, 10, 14, 17, 21, 24) and/or A1331852 (3 days per week starting on day 5) as indicated above. Photon flux analysis was performed as previously described [27].

393P cells (4×10^6) were injected subcutaneously into the flanks of 8–12 week old female Sv/129 mice. 393P tumors were allowed to grow for 6 days and then treated with vehicle, CM272 (5 days per week starting on day 6), anti-PD-1 (days 7, 10, 14, 17, 21, 24) and/or A1331852 (3 days per week starting on day 7) as indicated above.

Lacun.3 cells (1×10^6) were injected subcutaneously into the flanks of 8–12 week old female BALB/c mice. Lacun.3 tumors were allowed to grow for 13 days and then treated with vehicle, CM272 (5 days per week starting on day 13), anti-PD-1 (days 14, 17, 21, 24, 28, 31) and/or A1331852 (2 days per week starting on day 13) as indicated above.

B16.F10 cells (5×10^4) were injected subcutaneously into the flanks of 8–12 week old female C57BL/6 J mice and allowed to grow for 5 days. Mice were treated with vehicle, CM272 (5 days per week starting on day 5), anti-PD-1 (days 6, 9, 13, 16, 20) and/or A1331852 (3 days per week starting on day 5) as indicated above.

KPC cells (1×10^6) were injected subcutaneously into the flanks of 8–12 week old female C57BL/6 J mice and allowed to grow for 6 days. Tumor-bearing mice were treated with vehicle, CM272 (5 days per week starting on day 6), anti-PD-1 (days 7, 11, 14, 18, 21, 25, 28) and/or A1331852 (3 days per week starting on day 6) as indicated above.

MC38 cells (5×10^5) were injected subcutaneously into the flanks of 8–12 week old female C57BL/6 J mice and allowed to grow for 7 days. Mice were treated with vehicle, CM272 (5 days per week starting on day 7), anti-PD-1 (days 8 11, 15, 18) and/or A1331852 (3 days per week starting on day 7) as indicated above.

ANV5 cells (2×10^4) were injected orthotopically with Matrigel (1:1) through a 1 cm incision into the fourth and fifth inguinal mammary fat pads of 8–12 week old female FVB/N mice, as previously described [28]. ANV5 cells were allowed to grow for 7 days and then mice were treated with vehicle, CM272 (5 days per week starting on day 7), anti-PD-1 (days 8, 15) and/or A1331852 (3 days per week starting on day 7) as described above.

CT-2 A cells (5×10^3) were injected orthotopically into the caudate nucleus of 8–12 week old female C57BL/6 J mice, as previously described [29]. Tumors were allowed to grow for 6 days and then mice were treated with vehicle, CM272 (5 days per week starting on day 6), anti-PD-1 (days 7, 10, 14, 17, 21, 24) and/or A1331852 (3 days per week starting on day 6) as described above.

Humanized mouse model

A humanized mouse model was generated by retro-orbital intravenous injection of 1×10^7 fresh human peripheral blood mononuclear cells (PBMCs) into 6–8 week old NSG mice (The Jackson Laboratory) as previously described [30]. Briefly, HT29 human colon cancer cells (2×10^6 cells) were inoculated subcutaneously into the right flank of the mice seven days after the injection of PBMCs. HT29 cells were allowed to grow for 11 days and then mice were treated with vehicle, CM272 (5 days per week starting on day 11), 200 μg pembrolizumab (days 12, 15, 18) and/or A1331852 (3 days per week starting on day 11) as described in the previous section.

Immune cell depletion *in vivo*

Depletion of $CD8^+$, $CD4^+$ or natural killer (NK) cells was performed by intraperitoneal injection of 100 μg anti-mouse CD8α (clone 2.43; Bio X Cell), CD4 (clone GK1.5; Bio X Cell) or NK1.1 (clone PK136; Bio X Cell), respectively, as previously described [31].

Flow cytometry analysis of the TME

Single-cell suspensions of mouse tumors were obtained by mechanical and enzymatic dissociation using 1 mg/mL collagenase D (Roche) and 50 μg/mL DNase I (Roche) at 37 °C for 30 min. EDTA (6 μM) was then used to block collagenase and DNase I activities, and erythrocytes were removed as previously described [32]. The resulting single-cell suspensions were preincubated with Fc block for 15 min at 4°C, and then labeled for 15 min at 4°C with a fluorochrome-conjugated antibody cocktail diluted in FACS buffer. For intracellular staining, cells were fixed and permeabilized with fixation/permeabilization buffer (eBioscience) and labeled for intracellular markers in permeabilization buffer. The antibodies used are listed in Supplementary Table 3. Cell viability was assessed using PromoFluor 840 (1:2,560, Promokine). Cells were acquired using a Beckman Coulter CytoFLEX LX flow cytometer. Data were analyzed using FlowJo software (Tree Star). Gating strategies are shown in Supplementary Figs. 1 and 2.

Immunohistochemistry and multiplex immunofluorescence analysis

Paraffin-embedded 4-μm sections of lung tumors were used. PD-L1 detection by immunohistochemistry was performed following antigen retrieval in 10 mM citrate buffer (pH 6). The primary antibody, a rabbit anti-PD-L1 monoclonal antibody (Cell Signaling), was applied at

a 1:100 dilution. For quantification, slides were scanned using the Aperio CS2 scanner (Leica, Barcelona, Spain) and images were analyzed with QuPath v0.5.1. The H-score was subsequently calculated as described in previous studies [33].

Multispectral immunophenotyping was carried out according to the guidelines of Akoya Biosciences. Antibodies, antigen retrieval and dilutions for detection of CD4, CD8, F4/80, FoxP3 are shown in Supplementary Table 3. Autofluorescence control samples were included for validation. Samples were scanned using a Phenoimager HT system (Akoya), and spectral unmixing of signals was performed using InForm 2.5 (Akoya). Images were immunophenotyped using QuPath 0.5.0 [34]. Data were expressed as the number of cells with a specific immunophenotype divided by the total number of nucleated cells.

Single-cell transcriptomics

LLC tumors were injected and treated as described above. A total of 15 tumors (3 per treatment) were used for single-cell RNA sequencing (scRNA-seq). To manage sample numbers, LLC cells were injected into 5 mice on three consecutive days. Treatments with vehicle, CM2727, anti-PD-1, and/or A1331852 were performed as described above starting on day 7. On day 15, tumors were harvested and processed under sterile conditions as described above for flow cytometry. Erythrocytes were lysed as indicated above, and cells were resuspended in 35% Percoll solution (GE Healthcare) and centrifuged at 2,000 rpm for 15 min without brake. Afterwards, the supernatant was discarded and cells were preincubated with Fc block for 15 min at 4°C, and then labeled with fluorochrome-conjugated antibodies against CD45, CD11b and Ly6G (Supplementary Table 3). Dead cells were labeled with SYTOX Blue (Invitrogen). $CD45^+$ and double $CD11b^-/Ly6G^-$ cells were sorted. The transcriptome of the cells was sequenced using Single Cell 3'Reagent Kits v3.1 (10X Genomics). Briefly, 20,000 cells (except for sample 296_Triple, where only 5,840 cells could be obtained) were loaded at a concentration of 1,000 cells/µL on a Chromium X instrument (10X Genomics) to capture single cells in gel bead-in-emulsions (GEMs). In this step, each cell was encapsulated with primers containing a fixed Illumina Read 1 sequence, a cell-identifying 16 nt 10X barcode, a 12 nt unique molecular identifier (UMI), and a poly-dT sequence. After cell lysis, reverse transcription yielded full-length barcoded cDNA. This cDNA was then released from the GEMs, amplified by PCR and purified using magnetic beads (SPRIselect, Beckman Coulter). Enzymatic fragmentation and size selection were used to optimize cDNA size prior to library construction. Fragmented cDNA was then end-repaired, A-tailed and ligated to Illumina adaptors. A final PCR amplification with barcoded primers allowed for sample indexing. Library quality control and quantification were performed using the Qubit 3.0 Fluorometer (Life Technologies) and the 4200 TapeStation System (Agilent), respectively. Sequencing was performed on NextSeq2000 and NovaSeq6000 instruments (Illumina) (Read1: 28; Read2: 90; i7 index: 10; i5 index: 10) at an average depth of 20,000 reads/cell. Cell Ranger (v7.0.0, 10 × Genomics Inc) was used to align reads to the mouse genome (GRCm39) and generate gene-by-cell UMI count matrices. scRNA-seq computational guidelines [35] were followed using R packages (https://www.R-project.org/). Empty droplets were removed using DropleUtils 1.18.1 (FDR < 0.001). For quality control analysis, genes were filtered using SingleCellExperiment 1.20.1 based on the distribution of UMI reads, distribution of unique genes or > 5% of UMIs mapped to mitochondrial genes. scDblFinder [36] was used to identify and remove potential doublets. Genes with zero UMIs in all the cells were excluded from the analysis. Batchelor 1.14.1 [37] was used to mitigate potential batch effects. Normalization was performed using scuttle 1.8.4 [38]. Dimensionality reduction was performed using runPCA, runTSNE and runUMAP functions from scater 1.26.1 [38]. The Leiden community detection algorithm was applied to cluster the cells by performing clustering on a generated shared nearest neighbor (SNN) graph [39]. Clusters were manually annotated according to the expression of known cell-type marker genes. The ratio of observed to randomly expected cell numbers (Ro/e) was calculated for each cell type to assess the enrichment of cell subpopulations across treatments [40]. The expected cell number for each combination was obtained from the chi-squared test. Enriched cell subsets were characterized by a Ro/e > 1. Differentially expressed protein-coding genes were identified using a scalable implementation of the Wilcoxon rank sum test from presto 1.0.0. Genes with an adjusted p-value < 0.05 were considered to be differentially expressed. Gene set enrichment analysis (GSEA) was performed using fgsea 1.24.0 and the GO:BP (Gene Oncology: Biological Process) or KEGG gene sets. Genes were ranked by log2 FC. Scater 1.26.1 and ggplot2 3.5.1 were used to plot the data.

Statistical analyses

The statistical tests used to analyze the scRNA-seq data are described in the previous section. The Shapiro–Wilk test was used to determine the normal distribution of variables. Student's t-test and one-way ANOVA with Tukey's post hoc test were used to compare differences between two or more experimental groups, respectively. A p-value less than 0.05 was considered statistically

significant. GraphPad Prism 9 was used for statistical analysis and graphing.

Results

Co-targeting of epigenetic regulators and BCL-XL results in synergistic anti-tumor responses in human and mouse lung cancer cells

We first evaluated the effect of three representative epigenetic drugs, azacitidine (DNMT inhibitor), vorinostat (HDAC inhibitor) and CM272 (DNMT/HMT inhibitor), on a panel of human and mouse lung cancer cells. An increase in the expression of endogenous retroviruses (ERVs), helicases (MDA5 and RIGI) and IFN-stimulated genes (ISGs) was observed for the three drugs in all cell lines tested (Fig. 1A and B, and Supplementary Fig. 3). MDA5 and RIGI are sensors of RNA viruses in the cytosol and catalyze the hydrolysis of ATP upon binding to viral dsRNA [13, 41, 42]. Accordingly, a dose-dependent decrease in ATP was observed after treatment of lung cancer cells with CM272 (Fig. 1C). CM272 also induced an increase in oxygen consumption rate, suggesting an activation of OXPHOS (Fig. 1D). These results demonstrate that induction of ERV expression by epigenetic drugs switches cellular metabolism to OXPHOS in an attempt to compensate for ATP depletion. The switch to OXPHOS induced by epigenetic drugs may sensitize solid tumors to proapoptotic drugs that mediate mitochondrial-mediated death (Fig. 1E), as previously shown in hematological malignancies [23]. To evaluate this hypothesis, we incubated lung cancer cells with the epigenetic agent CM272 in combination with A1331852 (BCL-XL inhibitor), venetoclax (BCL2 inhibitor) or S63845 (MCL1 inhibitor) at different concentrations. While moderate synergism was observed in some cell lines treated in combination with BCL2 or MCL1 inhibitors, the combination with BCL-XL inhibition showed a strong synergistic effect in all tested human and mouse lung cancer cells (Fig. 1F and G, and Supplementary Figs. 4 and 5). The same effect was observed when the epigenetic drugs azacitidine or vorinostat were used in combination with the BCL-XL inhibitor (Supplementary Fig. 6). BCL-XL was the most abundant anti-apoptotic protein expressed by human and mouse lung cancer cell lines (Supplementary Fig. 7 A). Treatment with CM272 and the BCL-XL inhibitor did not alter anti-apoptotic protein expression in human cells but led to a reduction in BCL-XL and MCL1 levels in mouse cells (Supplementary Fig. 7B).

Next, we characterized the type of cell death induced by this combination. Flow cytometry analysis of Annexin V/propidium iodide (PI) staining revealed a marked increase in Annexin V and PI double-positive cells, indicative of late apoptosis, following combination treatment, whereas individual treatments had no such effect (Fig. 2A and Supplementary Fig. 8 A). Further analyses confirmed caspase-3-mediated apoptosis in the combination-treated cells (Fig. 2B, Supplementary Fig. 8B, and Fig. 2C). To assess whether the treatment induced an immunogenic cell death, we examined the translocation of calreticulin to the cell surface via flow cytometry. A notable increase in calreticulin-positive cells was observed following combination treatment (Fig. 2D). Accordingly, upregulation of PD-L1 and MHC-I expression was observed, further supporting the induction of immunogenic cell death (Supplementary Fig. 8 C). In conclusion, co-treatment of lung cancer cells with epigenetic agents and BCL-XL inhibition results in a broad synergistic anti-tumor effect associated with the induction of caspase-mediated apoptosis and immunogenic cell death. Notably, these results differ from data from hematological malignancies, which preferentially rely on BCL2, and to a lesser extent on MCL1, to prevent cell death [23].

(See figure on next page.)

Fig. 1 Epigenetic drug-mediated tumor cell death is enhanced by concomitant BCL-XL inhibition. **A**. Heatmap of the induced expression of endogenous retroviruses (ERVs), helicases and interferon-stimulated genes (ISGs) after treatment of human lung cancer cell lines with the epigenetic drug CM272. Expression was measured by real-time PCR. **B**. Heatmap of the induced expression of ERVs, helicases and ISGs after treatment of mouse lung cancer cell lines with the epigenetic drugs azacitidine, vorinostat or CM272. Expression was measured by real-time PCR. **C**. ADP/ATP ratio measured in human (A549, H460) and mouse (LLC, 393P) lung cancer cell lines treated with CM272 at IC_{50} and IC_{70}. **D**. Fold change in oxygen consumption rate (OCR) measured in human (A549, H460) and mouse (LLC, 393P) lung cancer cell lines treated with CM272 at IC_{50} and IC_{70}. **E**. Schematic representation of the synergistic anti-tumor effect of epigenetic and proapoptotic drugs. **F**. Combination index (CI) values and cell viability curves obtained after treatment of human (H226) and mouse (LLC) lung cancer cells with the epigenetic drug CM272 (at its IC_{50}) in combination with the proapoptotic drugs against BCL-XL (A1331852), BCL2 (venetoclax) or MCL-1 (S63845) at increasing concentrations. A synergistic effect between the two drugs was considered when at least four drug-drug interactions had CI values < 1. **G**. Relative IC_{50} values obtained when proapoptotic drugs were combined with the epigenetic drug CM272 (at its IC_{50}) in human and mouse lung cancer cell lines. Data are expressed as mean ± SEM. Student's t-test was used for statistical analysis in **C** and **D**

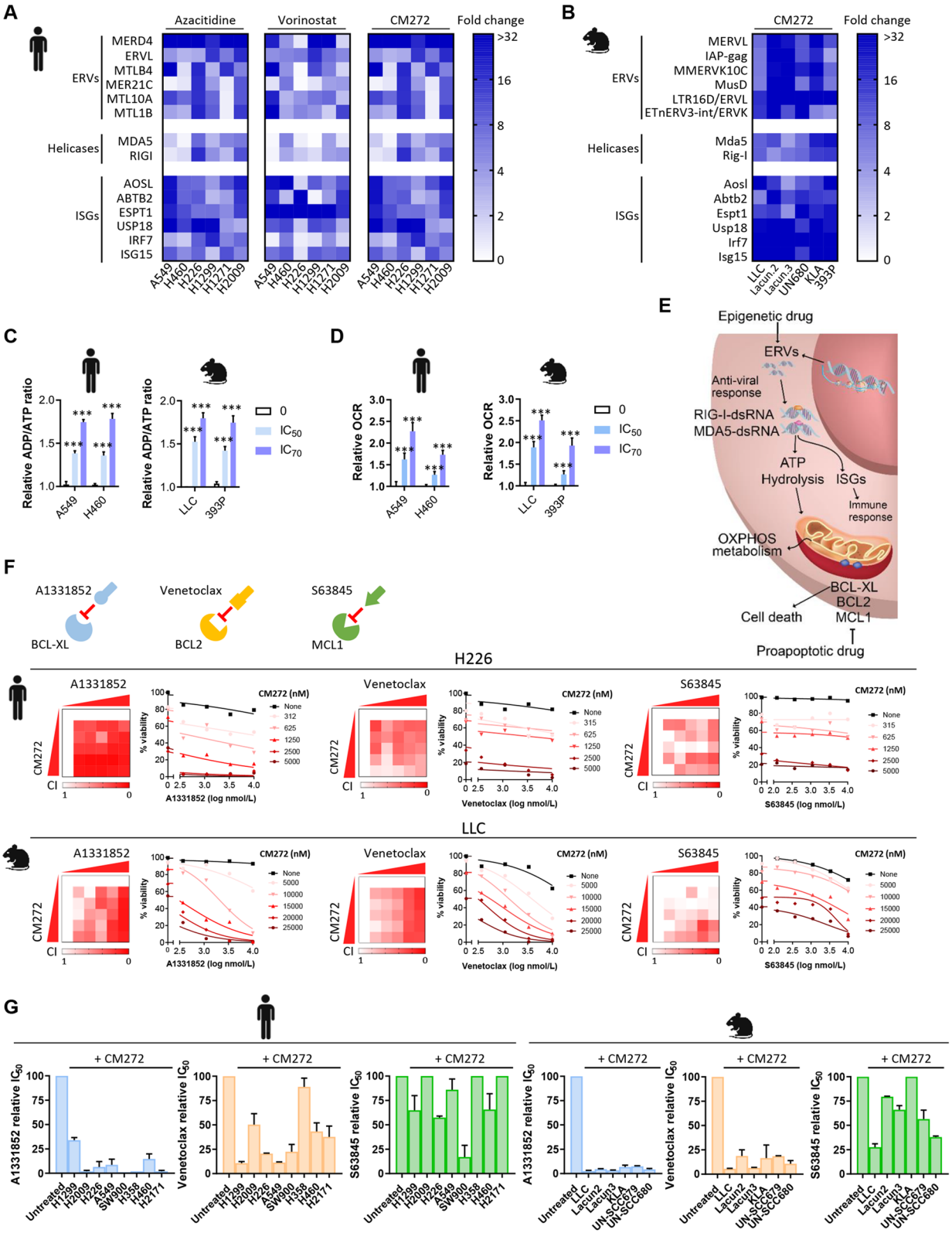

Fig. 1 (See legend on previous page.)

Combination of epigenetic drugs and BCL-XL inhibition sensitizes lung tumors to immune checkpoint blockade therapy

Co-treatment of lung cancer cells with epigenetic drugs and BCL-XL inhibition synergistically induced immunogenic cell death. Therefore, we hypothesized that this combination may enhance the efficacy of anti-PD-1/PD-L1 treatment against lung cancer cells (Fig. 3A). We tested this hypothesis using the epigenetic agent CM272, the BCL-XL inhibitor A1331852 and the anti-PD-1 monoclonal antibody RMP1-14 in three syngeneic lung cancer models based on subcutaneous inoculation of 393P, Lacun.3 or LLC cells (Fig. 3B and Supplementary Fig. 9 A).

In contrast to the in vitro data, double combinations of CM272/A1331852, CM272/anti-PD-1 or A1331852/anti-PD-1 showed little or no therapeutic effect. In contrast, the triple combination of CM272/A1331852/anti-PD-1 significantly reduced tumor growth and prolonged survival in the three models compared to the control groups (Fig. 3C). No differences in body weight were observed in treated mice compared to control mice (Supplementary Fig. 9B). We also tested the treatment in LLC-luc cells orthotopically inoculated into the lungs of syngeneic mice. LLC-luc tumors showed PD-L1 expression, which did not change with the treatment (Supplementary Fig. 9 C). On day 14 post-inoculation, bioluminescence image analysis showed a significant reduction in tumor burden in mice treated with the triple combination compared to the control group (Fig. 3D). Survival was significantly improved in treated mice, with complete regression in one mouse. From these experiments, we conclude that the combined treatment of an epigenetic drug with an anti-BCL-XL pro-apoptotic drug sensitizes lung cancer cells to immune checkpoint blockade.

Triple combination of an epigenetic agent, a BCL-XL inhibitor and an immune checkpoint inhibitor shows synergistic responses in multiple solid tumor types

To assess the relevance of our findings beyond lung cancer, we replicated some of the studies using cell lines from several types of solid tumors: melanoma, glioblastoma, colorectal cancer, breast cancer, and pancreatic cancer. Supplementary Fig. 10 A shows the ability of the epigenetic drug CM272 to induce the expression of ERVs, helicases and ISGs in different cell lines from these tumor types. As in lung cancer cells, BCL-XL was widely expressed in these cell lines (Supplementary Fig. 10B). In vitro synergistic studies with the epigenetic drug CM272 and the proapoptotic drugs A1331852, venetoclax and S63845 were performed in a broad panel of cancer cell lines of these origins. As previously observed in lung cancer, a strong synergy was observed for the combination of CM272 and the BCL-XL inhibitor A1331852 (Fig. 4A and 4B, Supplementary Figs. 11–15). Similar results were obtained with other epigenetic drugs (Supplementary Fig. 16).

The triple combination (CM272/A1331852/anti-PD-1) was then evaluated in vivo. In subcutaneous syngeneic pancreatic (KPC), colorectal (MC38), and melanoma (B16.F10) cancer models, the combination treatment significantly reduced tumor growth (Fig. 4C, 4D and 4E). In an orthotopic breast cancer model (ANV5), the therapeutic regimen also impaired tumor progression (Fig. 3F). Likewise, in a highly aggressive orthotopic glioblastoma model (CT-2 A), the treatment significantly prolonged survival (Fig. 4G). Finally, we tested the triple combination in a humanized colon cancer model based on the inoculation of HT-29 cells into NSG immunodeficient mice engrafted with human PBMCs (Fig. 4H). All treatment regimens showed a therapeutic effect, but the most significant response was seen with the triple combination, resulting in tumor regression in four out of five mice (Fig. 4H). In summary, the therapeutic efficacy of the combination of an epigenetic agent, a BCL-XL inhibitor and an immune checkpoint inhibitor represents a potential therapeutic option for many solid tumor types.

(See figure on next page.)

Fig. 2 A. Left panel: Representative Annexin V/PI staining of human (H460) and mouse (393P) lung cancer cells following treatment with the epigenetic drug CM272 and the BCL-XL inhibitor A1331852. Right panel: Quantification of late apoptotic cells (high Annexin V and PI staining) from three independent experiments. **B**. Representative activated caspase 3/7 and 7-ADD staining of human (H460) and mouse (393P) lung cancer cells following treatment with the epigenetic drug CM272 and the BCL-XL inhibitor A1331852. Right panel: Quantification of high active caspase 3/7 and 7-ADD staining from three independent experiments. **C**. Western blot analysis of caspase-3 cleavage in human and mouse lung cancer cell lines treated with CM272 and A1331852 alone or in combination. **D**. Calreticulin staining of human (H460 and A549) and mouse (393P and LLC) lung cancer cells following treatment with the epigenetic drug CM272 and the BCL-XL inhibitor A1331852. The graphs are representative of the results of two independent experiments. Treatment conditions were: H460: 5 μM CM272/2.5 μM A1331852; A549: 15 μM CM272, 5 μM A1331852; 393P and LLC: 30 μM CM272/2.5 μM A1331852. Cells were treated for 24 h. Data are presented as mean ± SEM. Statistical comparisons between treatment groups were conducted using one-way ANOVA followed by Tukey's post hoc test

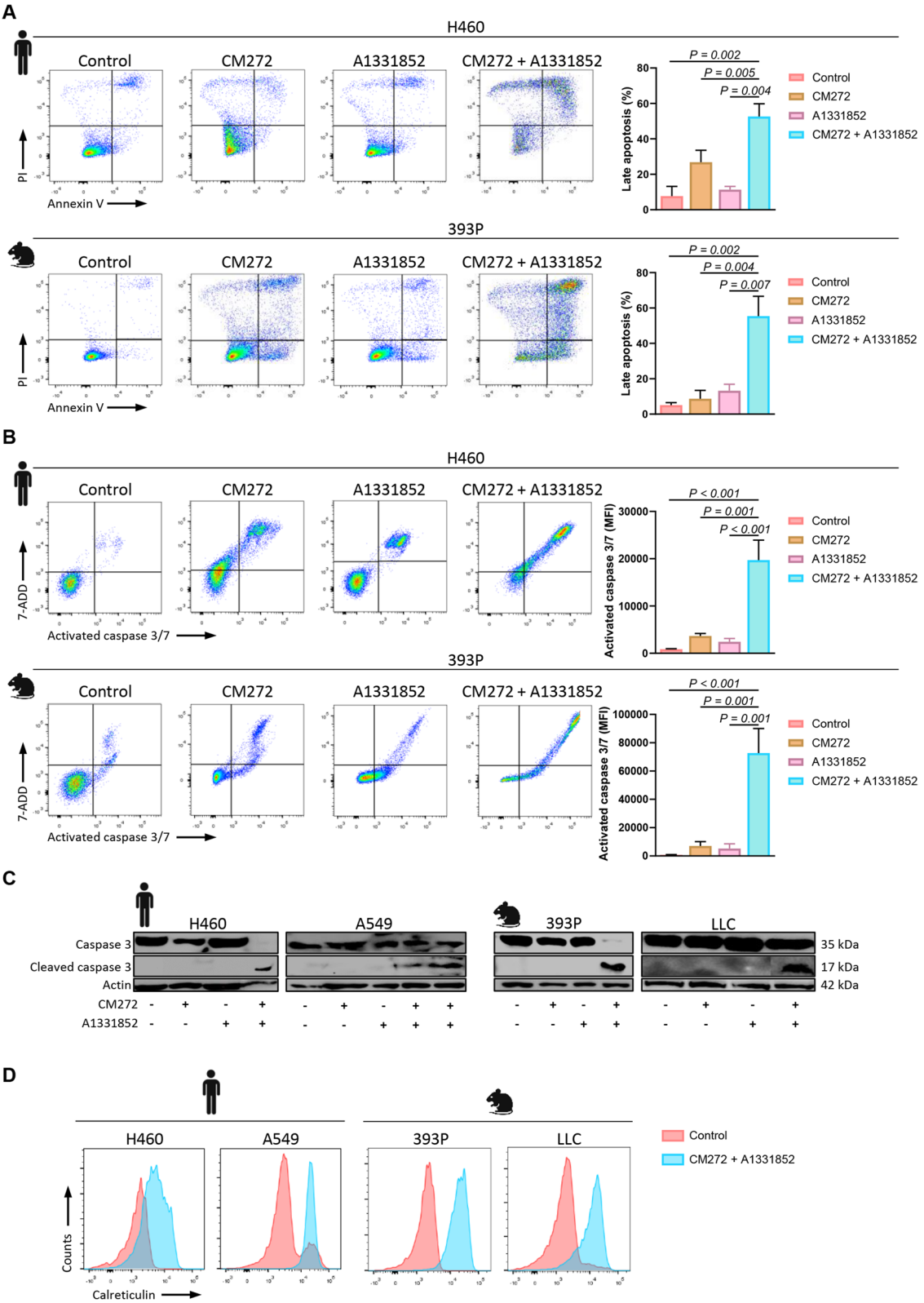

Fig. 2 (See legend on previous page.)

Triple combination therapy favors the anti-tumor activity of cytotoxic CD8 and NK cells by reducing the proportion of immunosuppressive cell subpopulations

To gain insight into the functional mechanisms underlying the anti-tumor activity of the triple combination, we first evaluated the contribution of CD8 T cells, CD4 T cells and NK cells by performing cell depletion experiments in vivo (Supplementary Fig. 17). In the LLC model, $CD8^+$ depletion abolished the anti-tumor activity of the triple combination, while $CD4^+$ depletion had no effect, and $NK1.1^+$ depletion had a moderate effect (Fig. 5A). Using flow cytometry, we analyzed the immune infiltrate in tumors treated with the different therapeutic regimens. In the lymphoid compartment, a significant decrease in T regulatory (Treg) cells was observed in tumors treated with the triple combination, together with a non-significant increase in CD8 T cells and NK cells and no differences in CD4 and B cells (Fig. 5B). No relevant differences in the expression of exhaustion markers (TIM-3, LAG-3 and GITR) in CD8, CD4 or NK cells were observed between treatments (Supplementary Fig. 18). In the myeloid compartment, the triple combination treatment significantly increased M1-like macrophages and the M1/M2 ratio. Dendritic cells (DCs) were reduced in the triple combination, but also in the double combination treatment based on CM272 and the BCL-XL inhibitor, monocytes showed a non-statistically significant increase and granulocytes in the triple combination showed similar levels to the control group (Fig. 5C). Similar results were obtained in 393P tumors concerning M1-like macrophages and the M1/M2 ratio, while no changes were observed in Treg cells (Supplementary Fig. 19). In the orthotopic LLC model, the tumor microenvironment (TME) was analyzed by multiplex immunophenotyping using two panels to evaluate T-cell and macrophage populations. Treg cells were reduced and M1-like macrophages were increased, although the latter change did not reach statistical significance (Fig. 5D). Overall, we conclude that the triple therapy induces an anti-tumor activity by promoting the cytotoxic functions of CD8 T cells and NK cells, reducing the immunosuppressive Treg cell population, and shifting the myeloid compartment toward a more pro-inflammatory phenotype characterized by an increase in M1-like macrophages and the M1/M2 ratio.

Single-cell characterization of TME changes induced by the triple combination CM272/A1331852/anti-PD-1

To further characterize the TME in the different treatment cohorts, we performed an scRNA-seq on hematopoietic cells ($CD45^+$) isolated from tumors treated with vehicle, the double combinations (CM272/A1331852, CM272/anti-PD-1 or A1331852/anti-PD-1) or the triple combination (CM272/A1331852/anti-PD-1). Neutrophils ($CD11b^+/Ly6G^+$) were excluded from this experiment because this subpopulation is present in high proportions in the TME, but no relevant differences were observed between treatments in the flow cytometry analysis. Cells were annotated as T cells, NK cells, B cells, monocytes/macrophages or DCs using canonical cell-type marker genes (Fig. 6A and Supplementary Fig. 20 A). In the triple combination, an increase in the number of NK cells and a decrease in the number of DCs was observed (Fig. 6B and Supplementary Fig. 20B). We then performed a subpopulation analysis of each cell type. Thirteen subtypes of T cells were identified (Fig. 6C and Supplementary Fig. 21 A). An increase in the frequency of exhausted CD4 T cells and cytotoxic CD8 T cells was observed in the triple combination compared to the other treatment regimens (Fig. 6D and Supplementary Fig. 21B). Interestingly, the frequency of a subpopulation of Treg cells decreased in tumors treated with the triple combination (Fig. 6D and Supplementary Fig. 21B). This subpopulation was annotated as effector Treg cells based on their higher expression of *Cd25* (*Il2ra*), *Foxp3* and *Ctla4* (Fig. 6E), as previously described [43]. Differential expression analysis identified *Ikzf2* (*Helios*) as one of the most significantly upregulated genes in this population (Supplementary Fig. 21 C). The expression of this gene has been associated with strong immunosuppressive properties in

(See figure on next page.)

Fig. 3 The epigenetic/proapoptotic drug combination CM272/A1331852 sensitizes lung tumors to anti-PD-1 therapy. **A**. Schematic representation of the hypothetical synergy between epigenetic drugs, BCL-XL inhibition and immunotherapy in vivo. **B**. Schematic representation of the therapeutic regimens followed in the cancer model based on subcutaneous inoculation of 393P lung cancer cells into syngeneic mice. The therapeutic regimens of the other models presented in this figure, Lacun.3 and LLC, are shown as supplementary material (Supplementary Fig. 9). C. Mice bearing 393P, Lacun.3 or LLC tumors were treated intraperitoneally with vehicle (control), CM272, A1331852 and/or anti-PD-1 as shown in **B**. Eight mice were used per group. Left panels: tumor size monitoring. Middle panels: tumor volumes on the last day of follow-up. Right panels: overall survival. **D.** Orthotopic LLC tumors treated with vehicle (control) or the triple combination (CM272/A1331852/anti-PD-1). Tumor growth was measured on day 14 after cell inoculation by bioluminescence (left) and presented as bio-layer interferometry (BLI) values (middle). Overall survival is shown in on the right. Eight mice were used in each group. Data are expressed as mean ± SEM. Comparisons between treatment strategies were performed by one-way ANOVA with Tukey's post hoc test, except for **D**, where Student's t-test was used. Survival curves were compared using the log rank test

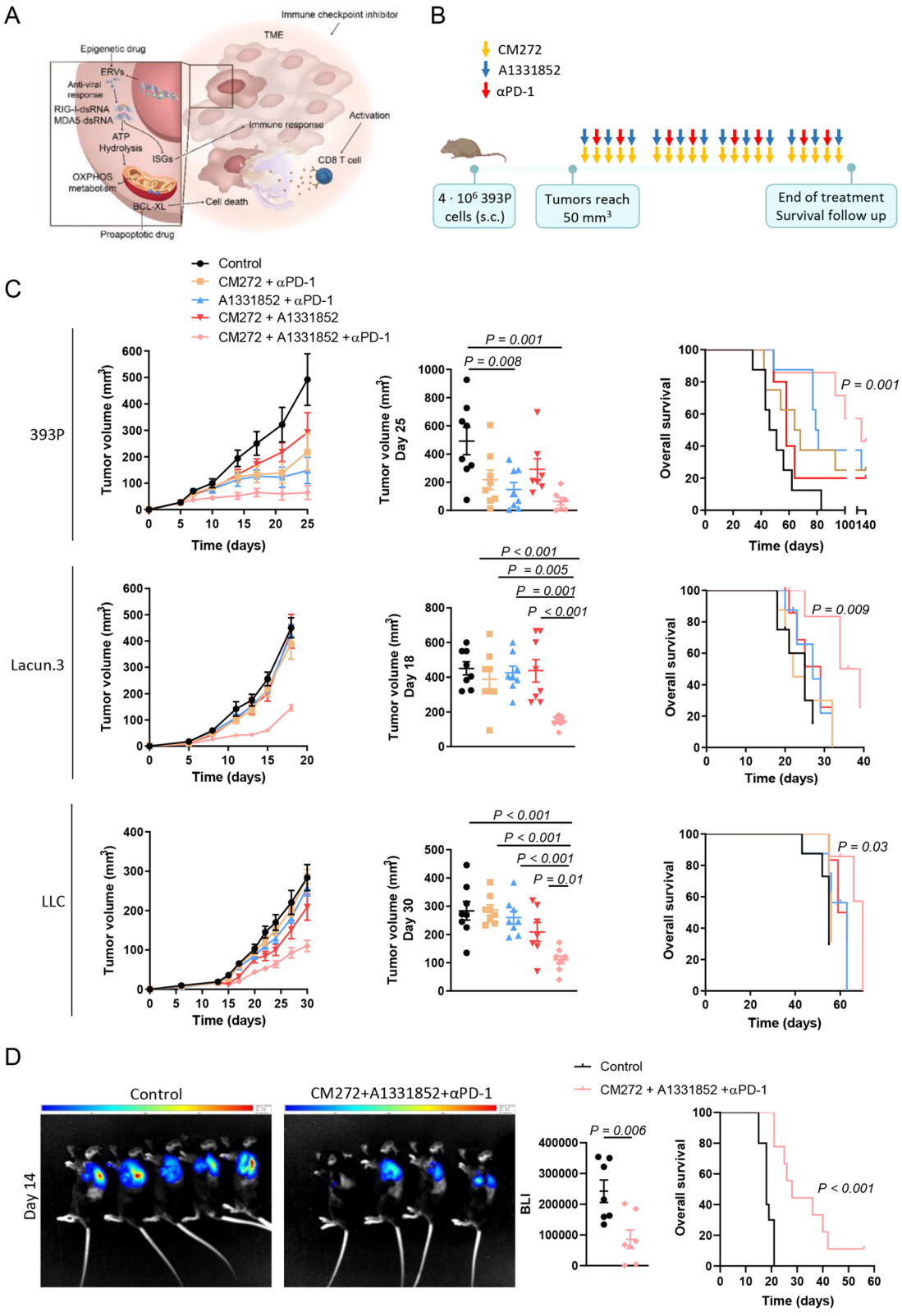

Fig. 3 (See legend on previous page.)

Treg cells [44]. *Itgb3*, a gene reported to promote cancer immune escape through TGF-β activation [45], was also upregulated in these cells, as were genes associated with thymic-derived lung resident Treg cells such as *Cd103* (*Itgae*), *Ikaros* (*Ikzf1*), *Il4r* or *Icos* [40, 41] (Fig. 6E). In the case of NK subtypes (Fig. 6F and Supplementary Fig. 22 A), the triple treatment was associated with a decrease in the frequency of immature NK cells and an increase in a subpopulation with high cytotoxic potential (Fig. 6G and Supplementary Fig. 22B), annotated as such by the expression of genes coding for perforin, granzyme A and B, and the regulator of cytotoxic granule exocytosis Nkg7 (Fig. 6H). Enrichment of genes belonging to the gene ontology (GO) cell killing pathway was also observed in these cells (Supplementary Fig. 22 C). Regarding B cell sub-clustering (Supplementary Fig. 23 A and 23B), a reduction in the presence of a subpopulation of mature B cells expressing high levels of *Bcl2* was observed in tumors treated with the triple combination compared to the control group and the double combinations (Supplementary Fig. 23 C and 23D). Compared to the other mature B cells in our study, this subpopulation showed a transcriptomic profile enriched in genes related to signaling pathways associated with cell survival and cancer (Supplementary Fig. 23E).

Regarding the myeloid compartment, monocytes/macrophages (Mo/MØs) were divided into six different sub-clusters (Fig. 6I and Supplementary Fig. 24 A). A drastic decrease in the frequency of two subpopulations was observed: *C1q*^{high} Mo/MØs and *Arg1*^{high} Mo/MØs (Fig. 6J and Supplementary Fig. 24B). Markers associated with an M2-like phenotype were preferentially expressed by these two subpopulations (Fig. 6K). With respect to DC subtypes (Fig. 6L and Supplementary Fig. 25 A), a decrease in a subpopulation of cDC2 s characterized by a high expression of *Dab2* was detected (Fig. 6M and Supplementary Fig. 25B). Dab2 is a negative regulator of DC immunogenicity that has been proposed as a target for DC-based immunotherapy [46]. This population also showed high expression levels of other tumor-promoting genes and genes associated with an immunosuppressive TME such as *Ifitm1*, *Tgfbi*, *Mif*, *Il1b* or its receptor *Il1r2* (Fig. 6N). In addition, this subpopulation showed the highest expression of class II transactivator (*Ciita*), the master regulator of MHC class II gene expression. Accordingly, these DCs expressed the highest levels of MHC class II genes and *Cd74*, a molecule essential for the assembly and subcellular trafficking of the MHC class II complex (Fig. 6N). This analysis suggests that *Dab-2*^{high} cDC2 s represent a DC subpopulation with immunosuppressive properties and high antigen presentation capacity.

In conclusion, the characterization of the immune cell populations affected by the triple combination CM272/A1331852/anti-PD-1 suggests that the anti-tumor effect of this treatment is mediated by the elimination of immune cells with immunosuppressive functions, such as effector Treg cells, M2-like macrophages, and *Dab2*^{high} cDC2 s, resulting in an increase of T and NK cells with cytotoxic potential.

Discussion

In this study, we demonstrate the utility of exploiting the cell-intrinsic death mechanism induced by the combination of epigenetic inhibitors and BH3 mimetics to sensitize solid tumors to ICB therapy. In particular, we propose the use of a triplet regimen combining a dual DNMT/HMT inhibitor (CM272) with a proapoptotic agent targeting BCL-XL and an anti-PD-1 monoclonal antibody. This multimodal combination effectively targets cancer cells by directly affecting cell viability and indirectly affecting the anti-tumor immune response. Our study demonstrates that this therapeutic strategy is applicable across a broad spectrum of solid cancers.

The proposed epigenetic regulator for our therapeutic combination was CM272, a small molecule that

(See figure on next page.)

Fig. 4 The epigenetic drug CM272 synergizes with proapoptotic drugs in vitro and in vivo in a variety of solid tumors. **A**. Reduction of IC_{50} of proapoptotic drugs against BCL-XL (A1331852), BCL2 (venetoclax) or MCL-1 (S63845) in combination with the epigenetic drug CM272 in human cancer cell lines of melanoma, glioblastoma, colorectal cancer, breast cancer and pancreatic cancer. **B**. Reduction of IC_{50} of proapoptotic drugs in combination with the epigenetic drug CM272 in mouse cancer cell lines of melanoma, glioblastoma, colorectal cancer, breast cancer and pancreatic cancer. **C**. Subcutaneous growth monitoring of KPC pancreatic tumors treated intraperitoneally with vehicle (control) or CM272 (five days per week), A1331852 (three days per week), and anti-PD-1 (two days per week). Eight mice were used in each group. **D**. Subcutaneous growth monitoring of MC38 colorectal tumors treated as above. **E**. Subcutaneous growth monitoring of B16.F10 melanoma tumors treated as above. **F**. Orthotopic growth monitoring of ANV5 breast tumors treated as above. **G.** Survival of mice bearing orthotopic CT-2 A glioblastomas treated as above. **H**. Left: humanized mouse model of subcutaneous HT-29 tumors. Right: percentage volume change from baseline at the end of the experiment is shown for each humanized mouse. Mice were treated with vehicle, CM272 (5 days per week starting on day 11), pembrolizumab (days 12, 15, 18), and/or A1331852. Five mice per group were used. Data are expressed as mean ± SEM. Comparisons between treatment strategies were carried out by Student's t-test analysis, except for **H**, where one-way ANOVA with Tukey's post hoc test was used. Survival curves were compared using the log rank test

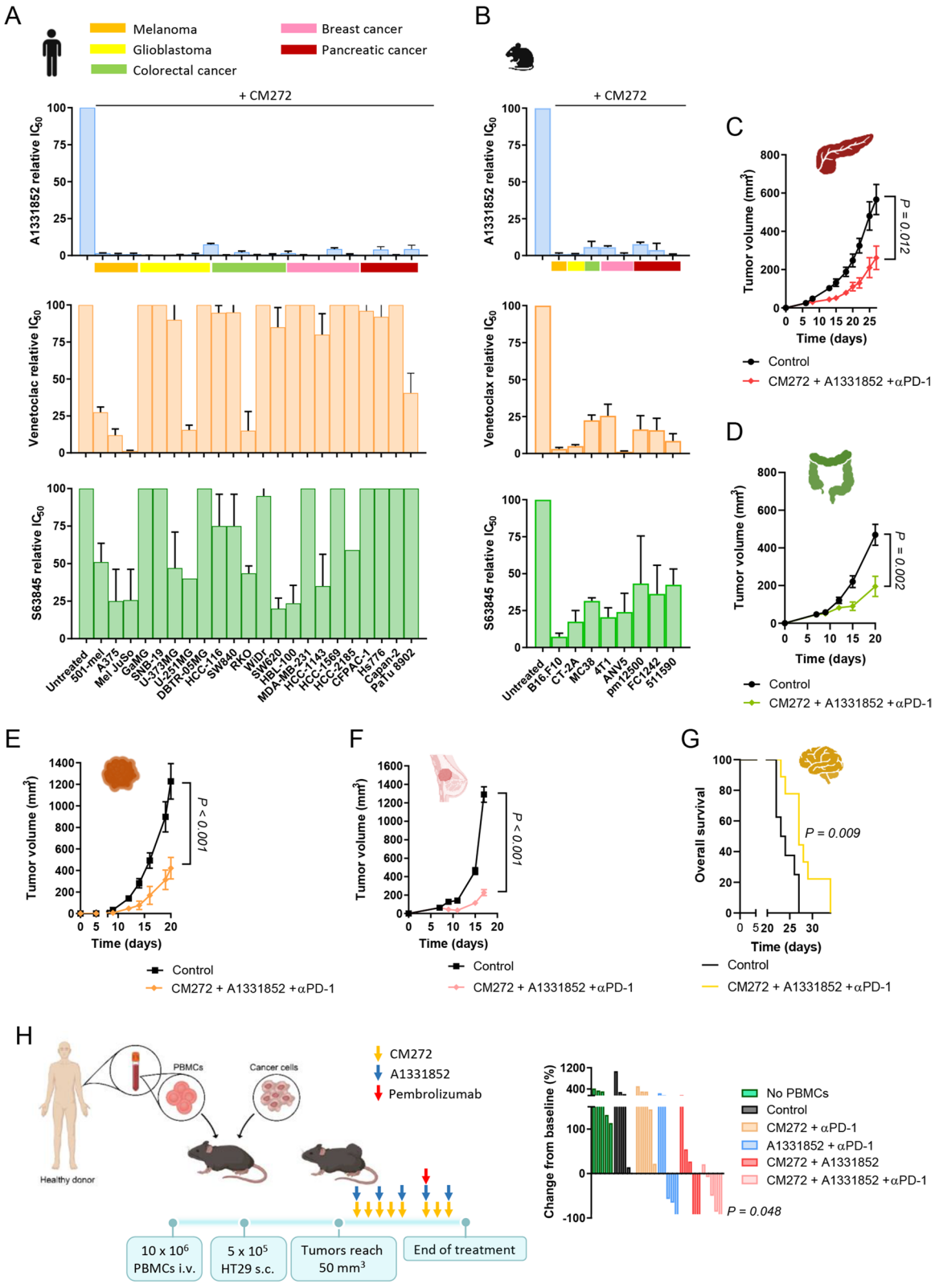

Fig. 4 (See legend on previous page.)

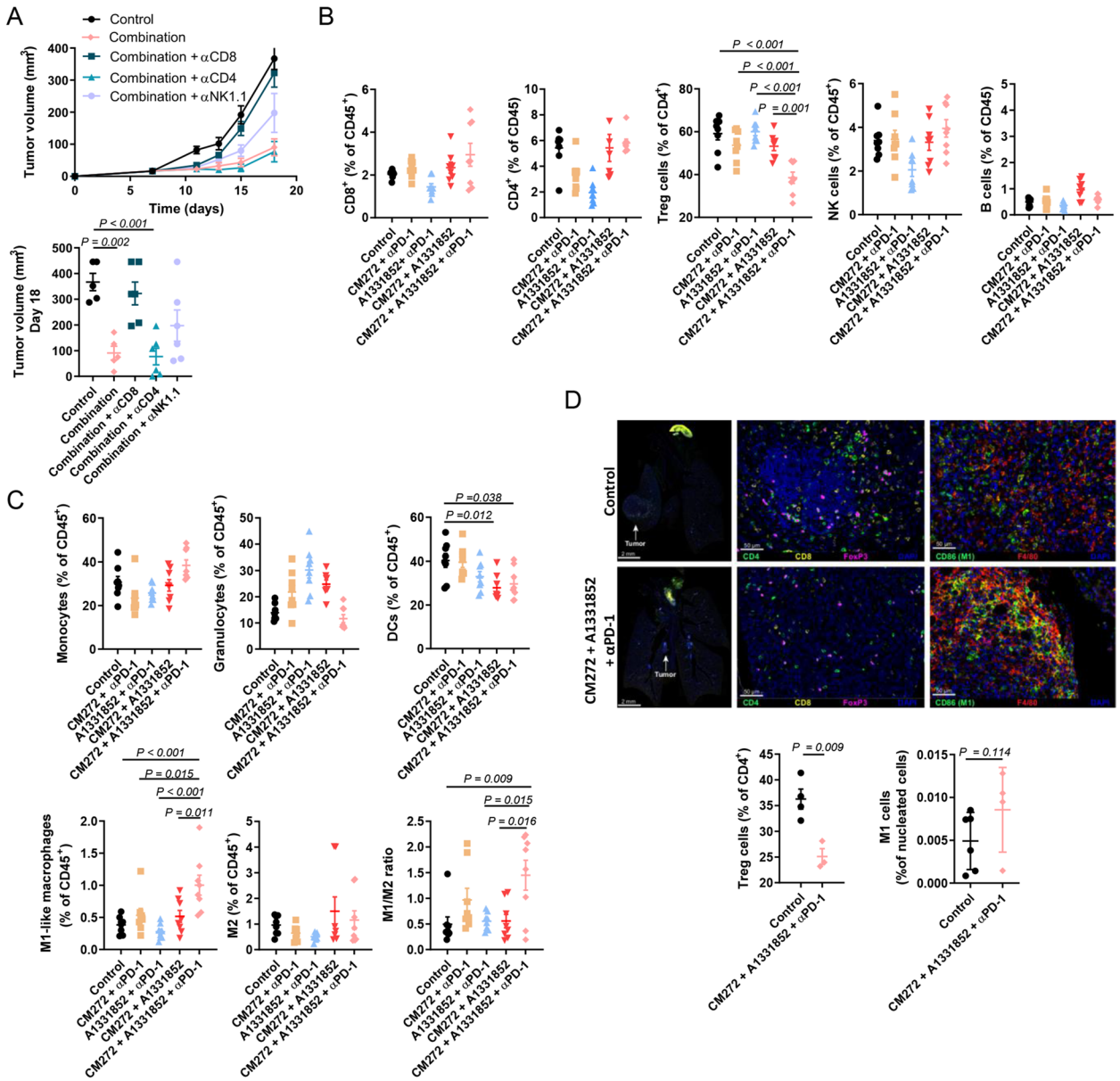

Fig. 5 The anti-tumor activity of the triple combination against lung tumors is associated with a reduction of immunosuppressive populations in the TME. **A**. LLC tumor-bearing mice were treated intraperitoneally with vehicle (control) or CM272 (five days per week)/A1331852 (three days per week)/anti-PD-1 (two days per week) in the presence or absence of the indicated depleting antibodies (days 6, 10, 14 and 18). Six mice were used per experimental group. Upper panel: follow-up of tumor size. Bottom panel: tumor volumes at the end of the experiment on day 18 post inoculation. **B**. Flow cytometry analysis of tumor-infiltrating lymphoid immune cells performed on day 15 after implantation of LLC cells in mice treated as above with vehicle (control), CM272, A1331852 and/or anti-PD-1. Eight mice were used per experimental group. Values are expressed as percentage of $CD45^+$ cells. Data are expressed as mean ± SEM. **C**. As in B, for cells in the myeloid compartment. **D**. Multiplex immunophenotyping in the orthotopic LLC tumors treated as above. Tumors were harvested at day 14 post-inoculation. Left: Representative merged immunofluorescence images for the quantification of CD4 (green), CD8 (yellow), FoxP3 (pink) and nucleus (DAPI) in panel 1; and CD86 (green), F4/80 (red) and nucleus (DAPI) in panel 2. Right: Quantification of Treg cells ($CD4^+$ $FoxP3^+$ cells) as a percentage of total $CD4^+$ cells and of M1-like macrophages ($F4/80^+$ $CD86^+$ cells). Comparisons were made by one-way ANOVA with Tukey's post hoc test in **A, B** and **C** and by Student's t-test in **D**

simultaneously targets G9a and DNMT1 [26]. This drug has been tested in diverse models of hematological and solid tumors, including hepatocellular carcinoma, pancreatic cancer, bladder cancer and lung cancer [26, 47–50]. In non-small cell lung cancer (NSCLC), elevated G9a and DNMT1 expression correlated with poor

prognosis, and their inhibition in experimental models has been shown to enhance the efficacy of diverse cancer therapies [47]. Epigenetic therapies, including CM272, trigger a common metabolic deregulation by transcriptionally activating endogenous retroelements, initiating viral mimicry responses that enhance tumor immunogenicity [8, 15–17, 50]. Here, we demonstrate that the combination of epigenetic regulators with BH3 mimetics, which inhibit prosurvival BCL2 family proteins, induces a potent anti-tumor activity in solid tumor cells, leading to immunogenic cell death. Clinical studies in hematological malignancies have shown that the efficacy of epigenetic drugs can be enhanced by apoptotic induction [25], and we have previously described the cell-intrinsic mechanism by which epigenetic inhibitors and BH3 mimetics act synergistically [23]. Notably, while hematological malignancies are primarily dependent on the anti-apoptotic proteins BCL2 and MCL1 to resist epigenetically induced metabolic stress, we found a striking sensitivity to BCL-XL inhibition across all tested solid tumors, both human and mouse. Previous studies have suggested a dependence of solid tumors on BCL-XL [51–53], although dependencies on other anti-apoptotic proteins have also been reported [54–60]. In our analysis, solid tumor cell lines exhibited higher BCL-XL expression compared to BCL2 or MCL1, consistent with their increased sensitivity to BCL-XL inhibition. While BCL-2 family proteins share similar functions, their binding patterns differ with respect to BH3-only proteins [61]. Therefore, tumor dependence on specific anti-apoptotic family members may also be influenced by the expression levels of activator BH3 proteins [62].

The potent anti-tumor activity of the combination of epigenetic drugs and BCL-XL inhibition observed in vitro in solid tumor cell lines did not translate in vivo, highlighting the influence of tumor cell-host interactions and raising concerns about the clinical efficacy of this approach. Inhibition of epigenetic regulators, such as HDACs, DNMTs or HMTs, can increase the immunogenicity of cancer cells through induction of dsRNA production from ERV genes and type I interferon response, leading to increased T-cell infiltration of tumors and synergistic effects with immune checkpoint blockade (ICB) [16, 23]. Proapoptotic drugs may also modulate immune cells [49, 63–66]. Therefore, we hypothesized that the strong immunogenic cell death induced by our dual epigenetic and pro-apoptotic intervention could enhance the effectiveness of ICB. Our findings confirmed this hypothesis. Using a broad range of preclinical solid tumor models, we demonstrate that the combination of the dual epigenetic inhibitor with a BCL-XL inhibitor and an anti-PD-1 antibody induces a synergistic anti-tumor response in vivo.

Our study also reveals that the therapeutic efficacy of combining the epigenetic and apoptotic modulation with ICB is closely tied to the immune response within the TME. Flow cytometry analysis of tumors treated with the epigenetic drug CM272 revealed a trend toward increased tumor-infiltrating CD8 T cells, an effect that was more pronounced when CM272 was combined with BCL-XL inhibition and ICB. Notable, the therapeutic benefit of this combination was completely lost upon $CD8^+$ T-cell depletion, demonstrating that the anti-tumor effects of the treatment are mediated by a CD8 T-cell response. This response was further associated with a reduction in immunosuppressive Treg cells, as well as an increase in M1-like macrophages and the M1/M2 ratio, suggesting a shift toward a more pro-inflammatory and tumor-suppressive immune environment.

Our scRNA-seq analysis provided a more comprehensive view of the immune subpopulation dynamics in response to treatment, revealing changes that were not captured by flow cytometry. We observed an increase in exhausted CD4 T cells in the triple combination group, suggesting sustained activation driven by the treatment-induced immune response. Another major effect, corroborating our flow cytometry findings, was a significant reduction in Treg cells following triple

(See figure on next page.)

Fig. 6 A scRNA-seq analysis reveals that the anti-tumor activity of the triple combination therapy is associated with a decrease in immunosuppressive subpopulations and an increase in cytotoxic subpopulations in the lymphoid and myeloid compartments of the TME. LLC tumor-bearing mice were treated with the triple combination CM272/A1331852/anti-PD-1. Three mice were used per experimental group. **A**. Two-dimensional t-distributed stochastic neighbor embedding (t-SNE) plot showing cell clusters of immune cells in the TME of LLC tumors. **B**. Prevalence of each cell type estimated by Ro/e score. **C**. t-SNE plot showing the sub-clusters of T cells. **D**. Prevalence of each T-cell subtype estimated by Ro/e score. **E**. Dot plot showing the expression of genes associated with effector or thymic-derived lung resident Treg cells. **F**. t-SNE plot showing the sub-clusters of NK cells. **G**. Prevalence of each NK subtype estimated by Ro/e score. **H**. Dot plot showing the expression of cytotoxic-associated genes in the sub-clusters of NK cells. **I**. t-SNE plot showing the sub-clusters of monocyte/macrophages (Mo/MØs). **J**. Prevalence of each subtype of Mo/MØs estimated by the Ro/e score. **K**. t-SNE plot showing the expression of genes associated with an M2 phenotype. **L**. t-SNE plot showing the sub-clusters of DCs. **M**. Prevalence of each subtype of DCs estimated by the Ro/e score. **N**. Dot plots showing the expression of genes associated with tumor promotion and immunosuppression (top panel), or the expression of genes associated with antigen presentation (bottom panel) in the sub-clusters of DCs

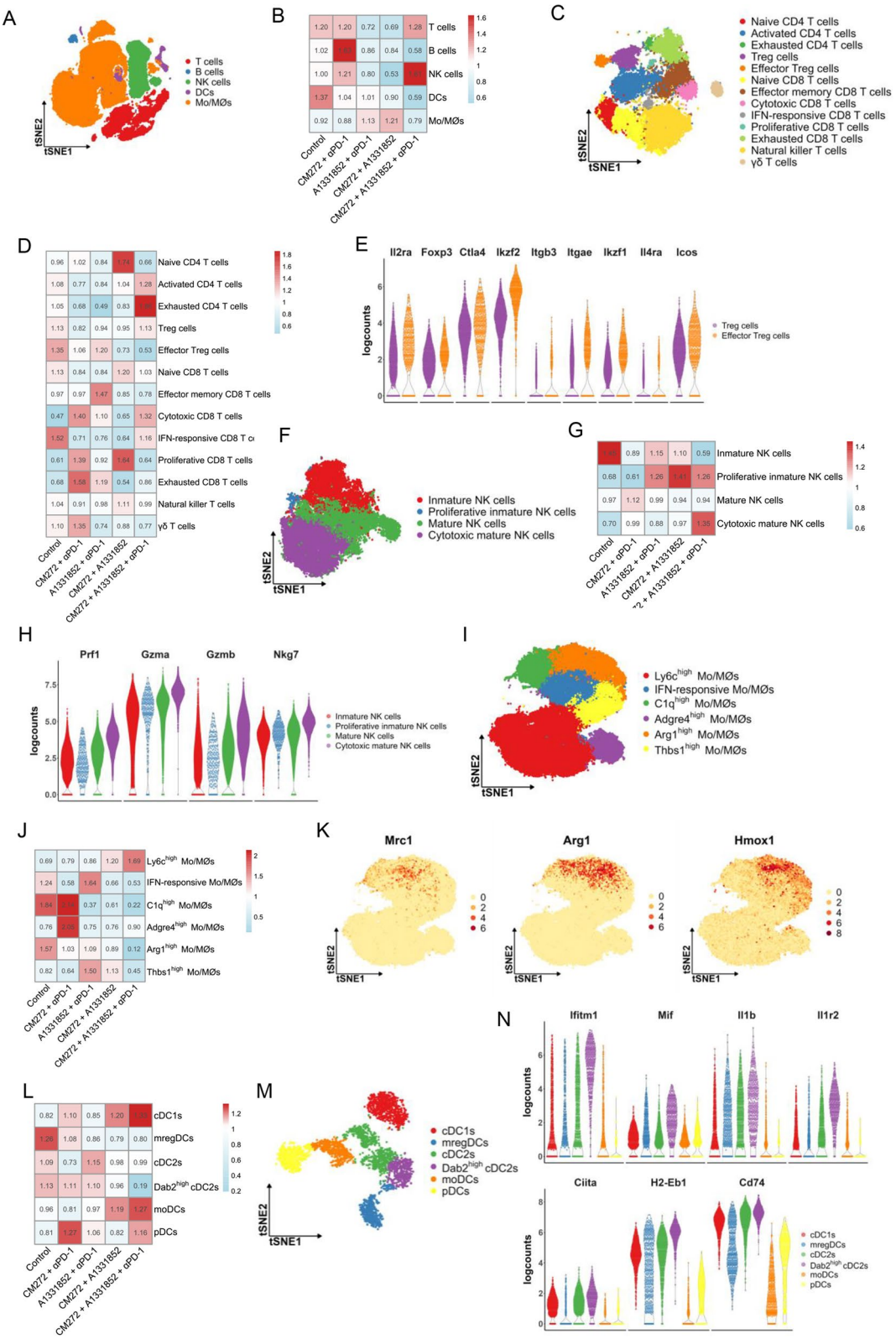

Fig. 6 (See legend on previous page.)

therapy. While BCL-XL inhibition has been reported to deplete intratumoral Treg cells [67], in our analysis, this effect was only evident when combined with epigenetic modulation and ICB. Specifically, the depleted Treg cell subset corresponded to thymus-derived, lung-resident Treg cells, a highly specialized immunosuppressive lineage characterized by strong Helios expression, along with the expression of immune checkpoint markers PD-1 and CTLA-4 [44, 68]. These cells, known for their ability to suppress virus-specific CD8 T cell responses [69], also exhibited upregulation of *Itgb3*, a gene implicated in cancer immune evasion via TGF-β signaling [45]. We also observed a reduction in a mature B cell subpopulation expressing high levels of Bcl-2, a gene linked to cancer progression by promoting cell survival in B cell malignancies [70]. In the myeloid compartment, the scRNA-seq analysis revealed a marked reduction in Mo/MØ subpopulations with an M2-like phenotype, characterized by high expression of *C1q* and *Arg1*. Additionally, we observed a decrease in a subset of cDC2 s expressing immunosuppressive-associated genes, including *Dab2*, *Ifitm1*, *Tgfbi*, *Mif*, *Il1b*, and its receptor *Il1r2*. This immune landscape reprogramming induced by the triple therapy is linked to the observed increase in the cytotoxic potential of CD8 T cells and NK cells, further highlighting the therapeutic potential of our combinatorial approach.

Our study lays the groundwork for the clinical evaluation of therapeutic strategies combining epigenetic modulation, BCL-XL inhibition and ICB. However, successful clinical translation requires careful assessment of potential toxicity risks. Although no changes in body weight were observed in treated mice, each component of the combination carries distinct safety concerns that warrant further evaluation. While epigenetic regulators may have off-target effects on normal cells, CM272 has demonstrated a favorable safety profile in previous in vivo studies, both alone and in combination with PD-1 blockade [49]. BCL-XL inhibitors are linked to thrombocytopenia due to their role in platelet survival, which may limit their clinical use [71, 72]. In addition, ICB carries a risk of immune-related adverse events. In this context, it is tempting to speculate that the synergistic drug interaction may allow for dose reductions of each individual agent while maintaining therapeutic efficacy. Reduced drug doses may alleviate toxicity concerns, such as thrombocytopenia from BCL-XL inhibition and immune-related adverse events from ICB. This dose-sparing potential strengthens the clinical feasibility of the combination. Further studies are needed to test this hypothesis and to optimize dosing strategies that maximize efficacy while minimizing toxicity.

In conclusion, the combination of epigenetic agents and BCL-XL inhibition exerts a broad anti-tumor effect that synergizes with ICB in in vivo preclinical cancer models of solid tumors. This therapeutic strategy enhances anti-tumor immunity by selectively eliminating immunosuppressive immune cells, thereby increasing the cytotoxic potential within the TME. Our findings highlight this approach as a promising therapeutic option for solid tumors, warranting further investigation for clinical translation.

Supplementary Information

The online version contains supplementary material available at https://doi.org/10.1186/s12943-025-02352-4.

Supplementary Material 1.

Supplementary Material 2.

Acknowledgements

The authors thank Silve Vicent (Program in Solid Tumors, Cima Universidad de Navarra) for providing 393P, KLA, LKR10, 511950, FC1242 and pm12500 cell lines, and Luis Montuenga (Program in Solid Tumors, Cima Universidad de Navarra) for providing Lacun.2, Lacun.3, UN-SCC679 and UN-SCC680 cell lines. This work was supported by Foundation for Applied Medical Research (FIMA), Centro de Investigación Biomédica en Red Cáncer (CIBERONC; CB16/12/00443 and CB16/12/00489), Spanish Ministry of Science, Innovation and Universities (PID2020-115875RBB-I00, PID2021-1226380B-100, PID2023-148573OB-I00 and PID2024-156335OB-I00), Instituto de Salud Carlos III (PI22/00983 and PI23/00573), co-funded by the European Union, Arnal Planelles Foundation, Jose Carreras Leukemia Foundation, Alberto Palatchi Foundation and AECC Foundation (PROYE20083LECA). Y.S. was funded by a predoctoral fellowship from the Spanish Ministry of Science, Innovation and Universities (FPU18/02638) and two mobility fellowships from University of Navarra and Government of Navarra. D.S. was funded by a Ramón y Cajal contract from the Spanish Ministry of Science, Innovation and Universities (RYC RYC2022-038084-I)

Authors' contributions

Y.S., V.F., V.J., J.A.M-C. and R.P. were responsible for the conception and design of the study. J.A.M-C. and R.P. supervised the study. Y.S., V.F., V.J., K.V., F.E., G.C., E.F-P., B.R-FC. M.G-H., A.R., H.M., D.S., D.A. performed in vitro and ex vivo experiments. P.SM-U. generated scRNAseq data. Y.S., I.T. and R.P. performed the analysis of scRNAseq data. K.V., M.M.A., F.L., A.P-L., F.L., M.F.S., A.C., J.A.M-C. and R.P. provided materials and resources, advised on the experimental design and interpreted the results. Y.S., V.F., V.J., J.A.M-C. and R.P. wrote the main manuscript text and prepared the figures. All authors critically reviewed the manuscript and approved the final version.

Data availability

The single-cell RNA sequencing data generated in this study are available in the Gene Expression Omnibus (GEO) repository (GSE288231). Additional data can be obtained upon reasonable request by contacting the corresponding authors.

Declarations

Competing interests

JAM-C received funding for research from Roche-Genentech, Bristol Myers Squibb-Celgene, Janssen, Regeneron, Priothera Pharmaceuticals, Palleon Pharmaceuticals, AstraZeneca, and K36 Therapeutics; is inventor on a patent 'Genetically engineered animal models for multiple myeloma' licensed to MIMO Biosciences; and is founder, holder of stock options, and royalties in MIMO Biosciences, all unrelated to this study. The other authors declare no conflict of interest.

The other authors declare no conflict of interest.

Author details
[1]Program in Solid Tumors, Cima Universidad de Navarra, Cancer Center Clínica Universidad de Navarra (CCUN), CIMA Building, Pio XII 55, 31008 Pamplona, Spain. [2]Navarra's Health Research Institute (IDISNA), Pamplona, Spain. [3]Department of Biochemistry and Genetics, School of Sciences, Universidad de Navarra, Pamplona, Spain. [4]Program in Hemato-Oncology, Cima Universidad de Navarra, CCUN, Pamplona, Spain. [5]Centro de Investigación Biomédica en Red Cáncer (CIBERONC), Madrid, Spain. [6]Department of Pathology, Anatomy and Physiology, Universidad de Navarra, Pamplona, Spain. [7]Department of Pediatrics, Clínica Universidad de Navarra, Pamplona, Spain. [8]Bioinformatics Platform, Cima Universidad de Navarra, Pamplona, Spain. [9]Enabling Technologies Division, Cima Universidad de Navarra, CCUN, Pamplona, Spain. [10]Hematology and Cell Therapy Area, CCUN, Pamplona, Spain. [11]Department of Oncology, CCUN, Pamplona, Spain.

Received: 17 January 2025 Accepted: 13 May 2025
Published online: 30 May 2025

References

1. Weiss AJ, Metter GE, Nealon TF, Keanan JP, Ramirez G, Swaiminathan A, Fletcher WS, Moss SE, Manthei RW. Phase II study of 5 azacytidine in solid tumors. Cancer Treat Rep. 1977;61:55–8.
2. Aparicio A, Eads CA, Leong LA, Laird PW, Newman EM, Synold TW, Baker SD, Zhao M, Weber JS. Phase I trial of continuous infusion 5-aza-2'-deoxycytidine. Cancer Chemother Pharmacol. 2003;51:231–9. https://doi.org/10.1007/S00280-002-0563-Y.
3. Samlowski WE, Leachman SA, Wade M, Cassidy P, Porter-Gill P, Busby L, Wheeler R, Boucher K, Fitzpatrick F, Jones DA, Karpf AR. Evaluation of a 7-day continuous intravenous infusion of decitabine: inhibition of promoter-specific and global genomic DNA methylation. J Clin Oncol. 2005;23:3897–905. https://doi.org/10.1200/JCO.2005.06.118.
4. Stewart DJ, Issa JP, Kurzrock R, Nunez MI, Jelinek J, Hong D, Oki Y, Guo Z, Gupta S, Wistuba II. Decitabine effect on tumor global DNA methylation and other parameters in a phase I trial in refractory solid tumors and lymphomas. Clin Cancer Res. 2009;15:3881–8. https://doi.org/10.1158/1078-0432.CCR-08-2196.
5. Feehley T, O'Donnell CW, Mendlein J, Karande M, McCauley T. Drugging the epigenome in the age of precision medicine. Clin Epigenetics. 2023;15:6. https://doi.org/10.1186/S13148-022-01419-Z.
6. Jin N, George TL, Otterson GA, Verschraegen C, Wen H, Carbone D, Herman J, Bertino EM, He K. Advances in epigenetic therapeutics with focus on solid tumors. Clin Epigenetics. 2021;13:83. https://doi.org/10.1186/S13148-021-01069-7.
7. Brocks D, Schmidt CR, Daskalakis M, Jang HS, Shah NM, Li D, Li J, Zhang B, Hou Y, Laudato S, Lipka DB, Schott J, Bierhoff H, Assenov Y, Helf M, Ressnerova A, Islam MS, Lindroth AM, Haas S, Essers M, Imbusch CD, Brors B, Oehme I, Witt O, Lübbert M, Mallm JP, Rippe K, Will R, Weichenhan D, Stoecklin G, Gerhäuser C, Oakes CC, Wang T, Plass C. DNMT and HDAC inhibitors induce cryptic transcription start sites encoded in long terminal repeats. Nat Genet. 2017;49:1052–60. https://doi.org/10.1038/NG.3889.
8. Chen R, Ishak CA, De Carvalho DD. Endogenous retroelements and the viral mimicry response in cancer therapy and cellular homeostasis. Cancer Discov. 2021;11:2707–25. https://doi.org/10.1158/2159-8290.CD-21-0506.
9. Chiappinelli KB, Strissel PL, Desrichard A, Li H, Henke C, Akman B, Hein A, Rote NS, Cope LM, Snyder A, Makarov V, Buhu S, Slamon DJ, Wolchok JD, Pardoll DM, Beckmann MW, Zahnow CA, Mergoub T, Chan TA, Baylin SB, Strick R. Inhibiting DNA methylation causes an interferon response in cancer via dsRNA including endogenous retroviruses. Cell. 2015;162:974–86. https://doi.org/10.1016/J.CELL.2015.07.011.
10. Deniz Ö, Frost JM, Branco MR. Regulation of transposable elements by DNA modifications. Nat Rev Genet. 2019;20:417–31. https://doi.org/10.1038/S41576-019-0106-6.
11. Ohtani H, Liu M, Zhou W, Liang G, Jones PA. Switching roles for DNA and histone methylation depend on evolutionary ages of human endogenous retroviruses. Genome Res. 2018;28:1147–57. https://doi.org/10.1101/GR.234229.118.
12. D. Roulois, H. Loo Yau, R. Singhania, Y. Wang, A. Danesh, S.Y. Shen, H. Han, G. Liang, P.A. Jones, T.J. Pugh, C. O'Brien, D.D. De Carvalho, DNA-demethylating agents target colorectal cancer cells by inducing viral mimicry by endogenous transcripts, Cell 2015 162;961–973. https://doi.org/10.1016/J.CELL.2015.07.056.
13. H. Kato, O. Takeuchi, S. Sato, M. Yoneyama, M. Yamamoto, K. Matsui, S. Uematsu, A. Jung, T. Kawai, K.J. Ishii, O. Yamaguchi, K. Otsu, T. Tsujimura, C.S. Koh, C. Reis E Sousa, Y. Matsuura, T. Fujita, S. Akira, Differential roles of MDA5 and RIG-I helicases in the recognition of RNA viruses. Nature 2006 441;101–105. https://doi.org/10.1038/NATURE04734.
14. Hou F, Sun L, Zheng H, Skaug B, Jiang QX, Chen ZJ. MAVS forms functional prion-like aggregates to activate and propagate antiviral innate immune response. Cell. 2011;146:448–61. https://doi.org/10.1016/J.CELL.2011.06.041.
15. M.J. Topper, M. Vaz, K.B. Chiappinelli, C.E. DeStefano Shields, N. Niknafs, R.W.C. Yen, A. Wenzel, J. Hicks, M. Ballew, M. Stone, P.T. Tran, C.A. Zahnow, M.D. Hellmann, V. Anagnostou, P.L. Strissel, R. Strick, V.E. Velculescu, S.B. Baylin, Epigenetic therapy ties MYC depletion to reversing immune evasion and treating lung cáncer. Cell 2017 171;1284–1300.e21. https://doi.org/10.1016/J.CELL.2017.10.022.
16. Sheng W, LaFleur MW, Nguyen TH, Chen S, Chakravarthy A, Conway JR, Li Y, Chen H, Yang H, Hsu PH, Van Allen EM, Freeman GJ, De Carvalho DD, He HH, Sharpe AH, Shi Y. LSD1 ablation stimulates anti-tumor immunity and enables checkpoint blockade. Cell. 2018;174:549-563.e19. https://doi.org/10.1016/J.CELL.2018.05.052.
17. Stone ML, Chiappinelli KB, Li H, Murphy LM, Travers ME, Topper MJ, Mathios D, Lim M, Shih IM, Wang TL, Hung CF, Bhargava V, Wiehagen KR, Cowley GS, Bachman KE, Strick R, Strissel PL, Baylin SB, Zahnow CA. Epigenetic therapy activates type I interferon signaling in murine ovarian cancer to reduce immunosuppression and tumor burden. Proc Natl Acad Sci U S A. 2017;114:E10981–90. https://doi.org/10.1073/PNAS.1712514114.
18. Keshari S, Barrodia P, Singh AK. Epigenetic perspective of immunotherapy for cancers. Cells. 2023;12:365. https://doi.org/10.3390/CELLS12030365.
19. Davalos V, Esteller M. Cancer epigenetics in clinical practice. CA Cancer J Clin. 2023;73:376–424. https://doi.org/10.3322/CAAC.21765.
20. A.N. Saltos, T. Tanvetyanon, B.C. Creelan, M. Rahman Shafique, S.J. Antonia, E.B. Haura, H. Zheng, X. Yu, J.J. Saller, S. Viracacha, R. Thapa, T.A. Boyle, D.-T. Chen, A.A. Beg, J.E. Gray, Phase II randomized trial of first-line pembrolizumab and vorinostat in patients with metastatic NSCLC (mNSCLC): Final results, J Clin Oncol 2023 41;9125.
21. US National Library of Medicine, https://www.clinicaltrials.gov/study/NCT03233724?term=epigenetic%20apoptosis&rank=10&tab=results, (n.d.).
22. B.P. Levy, G. Giaccone, B. Besse, E. Felip, M.C. Garassino, M. Domine Gomez, P. Garrido, B. Piperdi, S. Ponce-Aix, D. Menezes, K.J. MacBeth, A. Risueño, R. Slepetis, X. Wu, A. Fandi, L. Paz-Ares, Randomised phase 2 study of pembrolizumab plus CC-486 versus pembrolizumab plus placebo in patients with previously treated advanced non-small cell lung cancer, Eur J Cancer 2019 108;120–128. https://doi.org/10.1016/j.ejca.2018.11.028.
23. Fresquet V, Garcia-Barchino MJ, Larrayoz MJ, Celay J, Vicente C, Fernandez-Galilea M, Larrayoz MJ, Calasanz MJ, Panizo C, Junza A, Han J, Prior C, Fortes P, Pio R, Oyarzabal J, Martínez-Baztán Á, Paiva B, Moreno-Aliaga MJ, Odero MD, Agirre X, Yanes O, Prósper F, Martinez-Climent JA. Endogenous retroelement activation by epigenetic therapy reverses the Warburg effect and elicits mitochondrial-mediated cancer cell death. Cancer Discov. 2021;11:1268–85. https://doi.org/10.1158/2159-8290.cd-20-1065.
24. Singh R, Letai A, Sarosiek K. Regulation of apoptosis in health and disease: the balancing act of BCL-2 family proteins. Nat Rev Mol Cell Biol. 2019;20:175–93. https://doi.org/10.1038/S41580-018-0089-8.
25. DiNardo CD, Jonas BA, Pullarkat V, Thirman MJ, Garcia JS, Wei AH, Konopleva M, Döhner H, Letai A, Fenaux P, Koller E, Havelange V, Leber B, Esteve J, Wang J, Pejsa V, Hájek R, Porkka K, Illés Á, Lavie D, Lemoli RM, Yamamoto K, Yoon S-S, Jang J-H, Yeh S-P, Turgut M, Hong W-J, Zhou Y, Potluri J, Pratz KW. Azacitidine and venetoclax in previously untreated acute myeloid leukemia. N Engl J Med. 2020;383:617–29. https://doi.org/10.1056/NEJMOA2012971.
26. E. San José-Enériz, X. Agirre, O. Rabal, A. Vilas-Zornoza, J.A. Sanchez-Arias, E. Miranda, A. Ugarte, S. Roa, B. Paiva, A. Estella-Hermoso De Mendoza,

R.M. María Alvarez, N. Casares, V. Segura, J.I. Martín-Subero, F.X. Ogi, P. Soule, C.M. Santiveri, R. Campos-Olivas, G. Castellano, M. Garcia Fernandez De Barrena, J.R. Rodriguez-Madoz, M.J. García-Barchino, J.J. Lasarte, M.A. Avila, J.A. Martinez-Climent, J. Oyarzabal, F. Prosper, Discovery of first-in-class reversible dual small molecule inhibitors against G9a and DNMTs in hematological malignancies, Nat Commun 2017 8;15424. https://doi.org/10.1038/NCOMMS15424.

27. K. Valencia, C. Sainz, C. Bértolo, G. de Biurrun, J. Agorreta, A. Azpilikueta, M.J. Larrayoz, G. Bosco, C. Zandueta, M. Redrado, E. Redín, F. Exposito, D. Serrano, M. Echepare, D. Ajona, I. Melero, R. Pio, R. Thomas, A. Calvo, L.M. Montuenga, Two cell line models to study multiorganic metastasis and immunotherapy in lung squamous cell carcinoma, Dis Model Mech 2022 15;dmm049137. https://doi.org/10.1242/DMM.049137.
28. Ruiz-Fernández de Córdoba B, Moreno H, Valencia K, Perurena N, Ruedas P, Walle T, Pezonaga-Torres A, Hinojosa J, Guruceaga E, Pineda-Lucena A, Abengózar-Muela M, Cochonneau D, Zandueta C, Martínez-Canarias S, Teijeira Á, Ajona D, Ortiz-Espinosa S, Morales X, Ortiz de Solórzano C, Santisteban M, Ramos-García LI, Guembe L, Strnad V, Heymann D, Hervás-Stubbs S, Pío R, Rodríguez-Ruiz ME, de Andrea CE, Vicent S, Melero I, Lecanda F, Martínez-Monge R. Tumor ENPP1 (CD203a)/haptoglobin axis exploits myeloid-derived suppressor cells to promote post-radiotherapy local recurrence in breast cancer. Cancer Discov. 2022;12:1356–77. https://doi.org/10.1158/2159-8290.CD-21-0932.
29. Aldave G, Gonzalez-Huarriz M, Rubio A, Romero JP, Ravi D, Miñana B, Cuadrado-Tejedor M, García-Osta A, Verhaak R, Xipell E, Martinez-Vélez N, De La Rocha AA, Puigdelloses M, García-Moure M, Marigil M, Pérez-Larraya JG, Marín-Bejar O, Huarte M, Carro MS, Ferrarese R, Belda-Iniesta C, Ayuso A, Prat-Acín R, Pastor F, Díez-Valle R, Tejada S, Alonso MM. The aberrant splicing of BAF45d links splicing regulation and transcription in glioblastoma. Neuro Oncol. 2018;20:930–41. https://doi.org/10.1093/NEUONC/NOY007.
30. I. Eguren-Santamaria, E. Fernández de Piérola, G. Camps, P. Martín-Muñoz, M. Campos, D. Cuculescu, I. Aguilera-Buenosvinos, I. Rodríguez López, R. Salido-Vallejo, R. Alexandru, C.E. De Andrea, L. Álvarez-Gigli, P. Berraondo, I. Melero, M.F. Sanmamed, MHC class I and II-deficient humanized mice are suitable tools to test the long-term antitumor efficacy of immune checkpoint inhibitors and T-cell engagers, J Immunother Cancer 2024 12;e008516. https://doi.org/10.1136/JITC-2023-008516.
31. Ajona D, Ortiz-Espinosa S, Lozano T, Exposito F, Calvo A, Valencia K, Redrado M, Remírez A, Lecanda F, Alignani D, Lasarte JJ, Macaya I, Senent Y, Bértolo C, Sainz C, Gil-Bazo I, Eguren-Santamaría I, Lopez-Picazo JM, Gonzalez A, Perez-Gracia JL, de Andrea CE, Vicent S, Sanmamed MF, Montuenga LM, Pio R. Short-term starvation reduces IGF-1 levels to sensitize lung tumors to PD-1 immune checkpoint blockade. Nat Cancer. 2020;1:75–85. https://doi.org/10.1038/S43018-019-0007-9.
32. Ajona D, Ortiz-Espinosa S, Moreno H, Lozano T, Pajares MJ, Agorreta J, Bértolo C, Lasarte JJ, Vicent S, Hoehlig K, Vater A, Lecanda F, Montuenga LM, Pio R. A combined PD-1/C5a blockade synergistically protects against lung cancer growth and metastasis. Cancer Discov. 2017;7:694–703. https://doi.org/10.1158/2159-8290.CD-16-1184.
33. Villalba, Exposito, Pajares, Sainz, Redrado, Remirez, Wistuba, Behrens, Jantus-Lewintre, Camps, Montuenga, Pio, Lozano, de Andrea, Calvo, TMPRSS4: A novel tumor prognostic indicator for the stratification of stage IA tumors and a liquid biopsy biomarker for NSCLC patients, J Clin Med 2019 8;2134. https://doi.org/10.3390/jcm8122134
34. Bankhead P, Loughrey MB, Fernández JA, Dombrowski Y, McArt DG, Dunne PD, McQuaid S, Gray RT, Murray LJ, Coleman HG, James JA, Salto-Tellez M, Hamilton PW. QuPath: Open source software for digital pathology image analysis. Sci Rep. 2017;7:16878. https://doi.org/10.1038/S41598-017-17204-5.
35. Lun ATL, Riesenfeld S, Andrews T, Dao TP, Gomes T, Marioni JC. EmptyDrops: Distinguishing cells from empty droplets in droplet-based single-cell RNA sequencing data. Genome Biol. 2019;20:63. https://doi.org/10.1186/S13059-019-1662-Y.
36. P.L. Germain, M.D. Robinson, A. Lun, C. Garcia Meixide, W. Macnair, Doublet identification in single-cell sequencing data using scDblFinder, F1000Res 2022 10 979. https://doi.org/10.12688/F1000RESEARCH.73600.2/DOI.
37. Haghverdi L, Lun ATL, Morgan MD, Marioni JC. Batch effects in single-cell RNA-sequencing data are corrected by matching mutual nearest neighbors. Nat Biotechnol. 2018;36:421–7. https://doi.org/10.1038/NBT.4091.
38. McCarthy DJ, Campbell KR, Lun ATL, Wills QF. Scater: pre-processing, quality control, normalization and visualization of single-cell RNA-seq data in R. Bioinformatics. 2017;33:1179–86. https://doi.org/10.1093/BIOINFORMATICS/BTW777.
39. Traag VA, Waltman L, van Eck NJ. From Louvain to Leiden: Guaranteeing well-connected communities. Sci Rep. 2019;9:5233. https://doi.org/10.1038/S41598-019-41695-Z.
40. Zhang L, Yu X, Zheng L, Zhang Y, Li Y, Fang Q, Gao R, Kang B, Zhang Q, Huang JY, Konno H, Guo X, Ye Y, Gao S, Wang S, Hu X, Ren X, Shen Z, Ouyang W, Zhang Z. Lineage tracking reveals dynamic relationships of T cells in colorectal cancer. Nature. 2018;564:268–72. https://doi.org/10.1038/S41586-018-0694-X.
41. Yao H, Dittmann M, Peisley A, Hoffmann HH, Gilmore RH, Schmidt T, Schmid-Burgk JL, Hornung V, Rice CM, Hur S. ATP-dependent effector-like functions of RIG-I-like receptors. Mol Cell. 2015;58:541–8. https://doi.org/10.1016/J.MOLCEL.2015.03.014.
42. Peisley A, Lin C, Wu B, Orme-Johnson M, Liu M, Walz T, Hur S. Cooperative assembly and dynamic disassembly of MDA5 filaments for viral dsRNA recognition. Proc Natl Acad Sci U S A. 2011;108:21010–5. https://doi.org/10.1073/PNAS.1113651108/-/DCSUPPLEMENTAL/PNAS.1113651108_SI.PDF.
43. Tay C, Tanaka A, Sakaguchi S. Tumor-infiltrating regulatory T cells as targets of cancer immunotherapy. Cancer Cell. 2023;41:450–65. https://doi.org/10.1016/J.CCELL.2023.02.014.
44. A.S. Syed Khaja, S.M. Toor, H.E. Salhat, B.R. Ali, E. Elkord, Intratumoral FoxP3+Helios+ regulatory T cells upregulating immunosuppressive molecules Are expanded in human colorectal cancer, Front Immunol 2017 8;619. https://doi.org/10.3389/FIMMU.2017.00619.
45. Lainé A, Labiad O, Hernandez-Vargas H, This S, Sanlaville A, Léon S, Dalle S, Sheppard D, Travis MA, Paidassi H, Marie JC. Regulatory T cells promote cancer immune-escape through integrin αvβ8-mediated TGF-β activation. Nat Commun. 2021;12:6228. https://doi.org/10.1038/S41467-021-26352-2.
46. Ahmed MS, Byeon SE, Jeong Y, Miah MA, Salahuddin M, Lee Y, Park SS, Bae YS. Dab2, a negative regulator of DC immunogenicity, is an attractive molecular target for DC-based immunotherapy. Oncoimmunology. 2015;4:984550. https://doi.org/10.4161/2162402X.2014.984550.
47. F. Exposito, M. Redrado, D. Serrano, S. Calabuig-Fariñas, A. Bao-Caamano, S. Gallach, E. Jantus-Lewintre, A. Diaz-Lagares, A. Rodriguez-Casanova, J. Sandoval, E. San Jose-Eneriz, J. Garcia, E. Redin, Y. Senent, S. Leon, R. Pio, R. Lopez, J. Oyarzabal, A. Pineda-Lucena, X. Agirre, L.M. Montuenga, F. Prosper, A. Calvo, G9a/DNMT1 co-targeting inhibits non-small cell lung cancer growth and reprograms tumor cells to respond to cancer-drugs through SCARA5 and AOX1, Cell Death Dis 2024 15;787. https://doi.org/10.1038/S41419-024-07156-W.
48. M. Bárcena-Varela, S. Caruso, S. Llerena, G. Álvarez-Sola, I. Uriarte, M.U. Latasa, R. Urtasun, S. Rebouissou, L. Alvarez, M. Jimenez, E. Santamaría, C. Rodriguez-Ortigosa, G. Mazza, K. Rombouts, E. San José-Eneriz, O. Rabal, X. Agirre, M. Iraburu, A. Santos-Laso, J.M. Banales, J. Zucman-Rossi, F. Prósper, J. Oyarzabal, C. Berasain, M.A. Ávila, M.G. Fernández-Barrena, Dual targeting of histone methyltransferase G9a and DNA-methyltransferase 1 for the treatment of experimental hepatocellular carcinoma, Hepatology 2019 69;587–603. https://doi.org/10.1002/HEP.30168.
49. Oyon D, Lopez-Pascual A, Castello-Uribe B, Uriarte I, Orsi G, Llorente S, Elurbide J, Adan-Villaescusa E, Valbuena-Goiricelaya E, Irigaray-Miramon A, Latasa MU, Martinez-Perez LA, Bonetti LR, Prosper F, Ponz-Sarvise M, Vicent S, Pineda-Lucena A, Ruiz-Clavijo D, Sangro B, Larracoechea UA, Tian TV, Casadei-Gardini A, Amat I, Arechederra M, Berasain C, Urman JM, Avila MA, Fernandez-Barrena MG. Targeting of the G9a, DNMT1 and UHRF1 epigenetic complex as an effective strategy against pancreatic ductal adenocarcinoma. J Exp Clin Cancer Res. 2025;44:13. https://doi.org/10.1186/S13046-024-03268-5.
50. C. Segovia, E. San José-Enériz, E. Munera-Maravilla, M. Martínez-Fernández, L. Garate, E. Miranda, A. Vilas-Zornoza, I. Lodewijk, C. Rubio, C. Segrelles, L.V. Valcárcel, O. Rabal, N. Casares, A. Bernardini, C. Suarez-Cabrera, F.F. López-Calderón, P. Fortes, J.A. Casado, M. Dueñas, F. Villacampa, J.J. Lasarte, F. Guerrero-Ramos, G. de Velasco, J. Oyarzabal, D. Castellano, X. Agirre, F. Prósper, J.M. Paramio, Inhibition of a G9a/DNMT network triggers immune-mediated bladder cancer regression, Nat Med 2019 25;1073–1081. https://doi.org/10.1038/S41591-019-0499-Y.

51. Williams J, Lucas PC, Griffith KA, Choi M, Fogoros S, Hu YY, Liu JR. Expression of Bcl-xL in ovarian carcinoma is associated with chemoresistance and recurrent disease. Gynecol Oncol. 2005;96:287–95. https://doi.org/10.1016/j.ygyno.2004.10.026.
52. Scherr A-L, Mock A, Gdynia G, Schmitt N, Heilig CE, Korell F, Rhadakrishnan P, Hoffmeister P, Metzeler KH, Schulze-Osthoff K, Illert AL, Boerries M, Trojan J, Waidmann O, Falkenhorst J, Siveke J, Jost PJ, Bitzer M, Malek NP, Vecchione L, Jelas I, Brors B, Glimm H, Stenzinger A, Grekova SP, Gehrig T, Schulze-Bergkamen H, Jäger D, Schirmacher P, Heikenwalder M, Goeppert B, Schneider M, Fröhling S, Köhler BC. Identification of BCL-XL as highly active survival factor and promising therapeutic target in colorectal cancer. Cell Death Dis. 2020;11:875. https://doi.org/10.1038/s41419-020-03092-7.
53. Faqar-Uz-Zaman SF, Heinicke U, Meister MT, Vogler M, Fulda S. BCL-xL-selective BH3 mimetic sensitizes rhabdomyosarcoma cells to chemotherapeutics by activation of the mitochondrial pathway of apoptosis. Cancer Lett. 2018;412:131–42. https://doi.org/10.1016/j.canlet.2017.09.025.
54. Tan N, Malek M, Zha J, Yue P, Kassees R, Berry L, Fairbrother WJ, Sampath D, Belmont LD. Navitoclax enhances the efficacy of taxanes in non-small cell lung cancer models. Clin Cancer Res. 2011;17:1394–404. https://doi.org/10.1158/1078-0432.CCR-10-2353.
55. Xiao Y, Nimmer P, Sheppard GS, Bruncko M, Hessler P, Lu X, Roberts-Rapp L, Pappano WN, Elmore SW, Souers AJ, Leverson JD, Phillips DC. MCL-1 is a key determinant of breast cancer cell survival: validation of MCL-1 dependency utilizing a highly selective small molecule inhibitor. Mol Cancer Ther. 2015;14:1837–47. https://doi.org/10.1158/1535-7163.MCT-14-0928.
56. Zhang H, Guttikonda S, Roberts L, Uziel T, Semizarov D, Elmore SW, Leverson JD, Lam LT. Mcl-1 is critical for survival in a subgroup of non-small-cell lung cancer cell lines. Oncogene. 2011;30:1963–8. https://doi.org/10.1038/onc.2010.559.
57. Wacheck V, Cejka D, Sieghart W, Losert D, Strommer S, Crevenna R, Monia BP, Selzer E. Mcl-1 is a relevant molecular target for antisense oligonucleotide strategies in gastric cancer cells. Cancer Biol Ther. 2006;5:1348–54. https://doi.org/10.4161/cbt.5.10.3224.
58. Wei G, Margolin AA, Haery L, Brown E, Cucolo L, Julian B, Shehata S, Kung AL, Beroukhim R, Golub TR. Chemical genomics identifies small-molecule MCL1 repressors and BCL-xL as a predictor of MCL1 dependency. Cancer Cell. 2012;21:547–62. https://doi.org/10.1016/j.ccr.2012.02.028.
59. Munkhbaatar E, Dietzen M, Agrawal D, Anton M, Jesinghaus M, Boxberg M, Pfarr N, Bidola P, Uhrig S, Höckendorf U, Meinhardt A-L, Wahida A, Heid I, Braren R, Mishra R, Warth A, Muley T, Poh PSP, Wang X, Fröhling S, Steiger K, Slotta-Huspenina J, van Griensven M, Pfeiffer F, Lange S, Rad R, Spella M, Stathopoulos GT, Ruland J, Bassermann F, Weichert W, Strasser A, Branca C, Heikenwalder M, Swanton C, McGranahan N, Jost PJ. MCL-1 gains occur with high frequency in lung adenocarcinoma and can be targeted therapeutically. Nat Commun. 2020;11:4527. https://doi.org/10.1038/s41467-020-18372-1.
60. Kim MJ, Chen G, Sica GL, Deng X. Epigenetic modulation of FBW7/Mcl-1 pathway for lung cancer therapy. Cancer Biol Ther. 2021;22:55–65. https://doi.org/10.1080/15384047.2020.1856756.
61. K.J. Campbell, S.W.G. Tait, Targeting BCL-2 regulated apoptosis in cancer, Open Biol 2018 8. https://doi.org/10.1098/rsob.180002.
62. Inoue-Yamauchi A, Jeng PS, Kim K, Chen H-C, Han S, Ganesan YT, Ishizawa K, Jebiwott S, Dong Y, Pietanza MC, Hellmann MD, Kris MG, Hsieh JJ, Cheng EH. Targeting the differential addiction to anti-apoptotic BCL-2 family for cancer therapy. Nat Commun. 2017;8:16078. https://doi.org/10.1038/ncomms16078.
63. Hu X, Bardhan K, Paschall AV, Yang D, Waller JL, Park MA, Nayak-Kapoor A, Samuel TA, Abrams SI, Liu K. Deregulation of apoptotic factors Bcl-xL and Bax confers apoptotic resistance to myeloid-derived suppressor cells and contributes to their persistence in cancer. J Biol Chem. 2013;288:19103–15. https://doi.org/10.1074/JBC.M112.434530.
64. Carrington EM, Louis C, Kratina T, Hancock M, Keenan CR, Iannarella N, Allan RS, Wardak AZ, Czabotar PE, Herold MJ, Schenk RL, White CA, D'Silva D, Yang Y, Wong W, Wong H, Bryant VL, Huntington ND, Rautela J, Sutherland RM, Zhan Y, Hansen J, Nhu D, Lessene G, Wicks IP, Lew AM. BCL-XL antagonism selectively reduces neutrophil life span within inflamed tissues without causing neutropenia. Blood Adv. 2021;5:2550–62. https://doi.org/10.1182/BLOODADVANCES.2020004139.
65. Carrington EM, Zhang JG, Sutherland RM, Vikstrom IB, Brady JL, Soo P, Vremec D, Allison C, Lee EF, Fairlie WD, Bouillet P, Grabow S, Ottina E, Herold MJ, Pellegrini M, Huang DCS, Tarlinton DM, Strasser A, Lew AM, Zhan Y. Prosurvival Bcl-2 family members reveal a distinct apoptotic identity between conventional and plasmacytoid dendritic cells. Proc Natl Acad Sci U S A. 2015;112:4044–9. https://doi.org/10.1073/PNAS.1417620112.
66. Zhao L, Liu P, Mao M, Zhang S, Bigenwald C, Dutertre CA, Lehmann CHK, Pan H, Paulhan N, Amon L, Buqué A, Yamazaki T, Galluzzi L, Kloeckner B, Silvin A, Pan Y, Chen H, Tian AL, Ly P, Dudziak D, Zitvogel L, Kepp O, Kroemer G. BCL2 inhibition reveals a dendritic cell-specific immune checkpoint that controls tumor immunosurveillance. Cancer Discov. 2023;13:2448–69. https://doi.org/10.1158/2159-8290.CD-22-1338.
67. Kolb R, De U, Khan S, Luo Y, Kim MC, Yu H, Wu C, Mo J, Zhang X, Zhang P, Zhang X, Borcherding N, Koppel D, Fu YX, Zheng SG, Avram D, Zheng G, Zhou D, Zhang W. Proteolysis-targeting chimera against BCL-XL destroys tumor-infiltrating regulatory T cells. Nat Commun. 2021;12:1281. https://doi.org/10.1038/S41467-021-21573-X.
68. A.S. Syed Khaja, S.M. Toor, H. El Salhat, I. Faour, N. ul Haq, B.R. Ali, E. Elkord, Preferential accumulation of regulatory T cells with highly immunosuppressive characteristics in breast tumor microenvironment, Oncotarget 2017 8;33159–33171. https://doi.org/10.18632/ONCOTARGET.16565.
69. Lu C, Chen W. Influenza virus infection selectively triggers the accumulation and persistence of more potent Helios-expressing Foxp3+ regulatory T cells in the lungs. Immunol Cell Biol. 2021;99:1011–25. https://doi.org/10.1111/IMCB.12492.
70. Kapoor I, Bodo J, Hill BT, Hsi ED, Almasan A. Targeting BCL-2 in B-cell malignancies and overcoming therapeutic resistance. Cell Death Dis. 2020;11:941. https://doi.org/10.1038/S41419-020-03144-Y.
71. Rudin CM, Hann CL, Garon EB, Ribeiro De Oliveira M, Bonomi PD, Camidge DR, Chu Q, Giaccone G, Khaira D, Ramalingam SS, Ranson MR, Dive C, McKeegan EM, Chyla BJ, Dowell BL, Chakravartty A, Nolan CE, Rudersdorf N, Busman TA, Mabry MH, Krivoshik AP, Humerickhouse RA, Shapiro GI, Gandhi L. Phase II study of single-agent navitoclax (ABT-263) and biomarker correlates in patients with relapsed small cell lung cancer. Clin Cancer Res. 2012;18:3163–9. https://doi.org/10.1158/1078-0432.CCR-11-3090.
72. Schoenwaelder SM, Jarman KE, Gardiner EE, Hua M, Qiao J, White MJ, Josefsson EC, Alwis I, Ono A, Willcox A, Andrews RK, Mason KD, Salem HH, Huang DCS, Kile BT, Roberts AW, Jackson SP. Bcl-xL-inhibitory BH3 mimetics can induce a transient thrombocytopathy that undermines the hemostatic function of platelets. Blood. 2011;118:1663–74. https://doi.org/10.1182/BLOOD-2011-04-347849.

Publisher's Note

Springer Nature remains neutral with regard to jurisdictional claims in published maps and institutional affiliations.